



HAL
open science

3-Benzylmenadiones and their Heteroaromatic Analogues Target the Apicoplast of Apicomplexa Parasites: Synthesis and Bioimaging Studies

Baptiste Dupouy, Maxime Donzel, Matthieu Roignant, Sarah Charital, Rodrigue Keumoe, Yoshiki Yamaryo-Botté, Alexander Feckler, Mirco Bundschuh, Yann Bordat, Matthias Rottmann, et al.

► To cite this version:

Baptiste Dupouy, Maxime Donzel, Matthieu Roignant, Sarah Charital, Rodrigue Keumoe, et al.. 3-Benzylmenadiones and their Heteroaromatic Analogues Target the Apicoplast of Apicomplexa Parasites: Synthesis and Bioimaging Studies. *ACS Infectious Diseases*, 2024, 10 (10), pp.3553-3576. 10.1021/acsinfecdis.4c00304 . hal-04728547

HAL Id: hal-04728547

<https://hal.science/hal-04728547v1>

Submitted on 9 Oct 2024

HAL is a multi-disciplinary open access archive for the deposit and dissemination of scientific research documents, whether they are published or not. The documents may come from teaching and research institutions in France or abroad, or from public or private research centers.

L'archive ouverte pluridisciplinaire **HAL**, est destinée au dépôt et à la diffusion de documents scientifiques de niveau recherche, publiés ou non, émanant des établissements d'enseignement et de recherche français ou étrangers, des laboratoires publics ou privés.

3-benzylmenadiones and their heteroaromatic analogues target the apicoplast of Apicomplexa parasites: Synthesis and bioimaging studies

Baptiste Dupouy,^{1,#} Maxime Donzel,^{1,#} Matthieu Roignant,^{1,#} Sarah Charital,² Rodrigue Keumoe,³ Yoshiki Yamaro-Botté,² Alexander Feckler,⁴ Mirco Bundschuh,⁴ Yann Bordat,⁵ Matthias Rottmann,⁶ Pascal Mäser,^{6,7} Cyrille Y. Botté,² Stéphanie A. Blandin,³ Sébastien Besteiro,⁵ Elisabeth Davioud-Charvet^{*,1}

authors contributed equally as first co-authors

* Correspondence E-mail Address: elisabeth.davioud@unistra.fr

¹ UMR7042 CNRS-Unistra-UHA, Laboratoire d'Innovation Moléculaire et Applications (LIMA), Bio(in)organic & Medicinal Chemistry Team, European school of Chemistry, Polymers and Materials (ECPM), 25, rue Becquerel, F-67087 Strasbourg, France.

² Apicolipid Team, Institut pour l'Avancée des Biosciences, CNRS UMR5309,INSERM U1209, Université Grenoble Alpes, Bat. Jean Roget, Domaine de la Merci, F-38700 La Tronche, France.

³ INSERM, CNRS, Université de Strasbourg, U1257 / UPR9022, Mosquito Immune Responses IBMC, 2 Allée Konrad Roentgen, F-67000 Strasbourg, France.

⁴ Functional Aquatic Ecotoxicology, Institute for Environmental Sciences (iES), RPTU Kaiserslautern-Landau, Fortstrasse 7, D-76829 Landau, Germany

⁵ UMR5294 CNRS-Université de Montpellier, Laboratory of Pathogens and Host Immunity (LPHI), Place Eugène Bataillon, Bâtiment 24, CC 107, F-34095 Montpellier cedex 5, France.

⁶ Swiss Tropical and Public Health Institute, Kreuzstrasse 2, CH-4123 Allschwil, Switzerland.

⁷ University of Basel, Petersgraben 1, CH-4001 Basel, Switzerland.

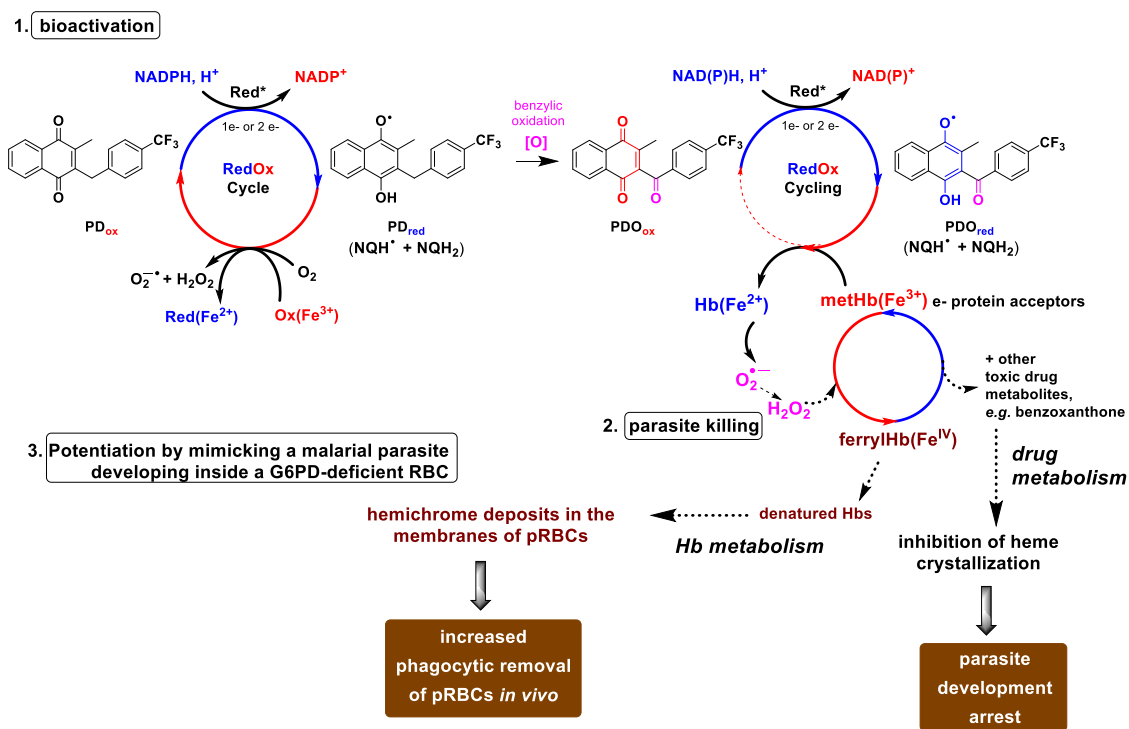
ABSTRACT:

The apicoplast is an essential organelle for the viability of apicomplexan parasites *Plasmodium falciparum* or *Toxoplasma gondii*, which has been proposed as a suitable drug target for the development of new antiplasmodial drug-candidates. Plasmodione, an antimalarial redox-active lead drug is active at low nM concentrations on several blood stages of *Plasmodium* such as early rings and gametocytes. Nevertheless, its precise biological targets remain unknown. Here, we described the synthesis and the evaluation of new heteroaromatic analogues of plasmodione, active on asexual blood *P. falciparum* stages and *T. gondii* tachyzoites. Using a bioimaging-based analysis, we followed the morphological alterations of *T. gondii* tachyzoites and revealed a specific loss of the apicoplast upon drug treatment. Lipidomic and fluxomic analyses determined that drug treatment severely impacts apicoplast-hosted FASII activity in *T. gondii* tachyzoites, further supporting that the apicoplast is a primary target of plasmodione analogues. To follow the drug localization, 'clickable' analogues of plasmodione were designed as tools for fluorescence imaging through a Cu(I)-catalyzed Azide-Alkyne Cycloaddition reaction. Short-time incubation of two probes with *P. falciparum* trophozoites and *T. gondii* tachyzoites showed that the clicked products localize within, or in the vicinity of, the apicoplast of both Apicomplexa parasites. In *P. falciparum* the fluorescence signal was also associated with the mitochondrion, suggesting that bioactivation and activity of plasmodione and related analogues are potentially associated to these two organelles in malaria parasites.

KEYWORDS: apicoplast, CuAAC-based imaging, lipidomics, plasmodione, *Plasmodium falciparum*, *Toxoplasma gondii*

Collectively, parasites of the phylum Apicomplexa are responsible for widespread life-threatening diseases of human and cattle with major human and economic consequences. The most devastating of these is Malaria, a major tropical parasitic disease that was responsible for 249 million human cases and 608,000 deaths worldwide in 2022, mostly affecting young children below the age of 8 in Sub-Saharan Africa (1). *Plasmodium* is the causative agent of malaria, the most lethal species being *P. falciparum*, which is responsible for malaria complications such as cerebral malaria or severe anemia. Resistance to artemisinin (ART-R), alone or in combination therapies also known as ACTs, has emerged in southeast Asia, and in the last decade multidrug-resistance of *Plasmodium* toward broadly-used antimalarial drugs has spread all over the world. About 95% of cases and deaths are located in Africa, with young children and pregnant women particularly at risk. At the molecular level, ART-R is principally linked to a subset of about 20 mutations in the propeller domain of *P. falciparum* kelch13 (*PfK13*) protein. However, in the past few years, multiple independent emergences of *PfK13* mutations have been associated with multidrug resistance, and in some area, decreased ACT efficacy was found independent of *PfK13* mutations in Africa. The emergence of ART-R in Africa has thus generated a high concern regarding the loss of efficacy of ACT partner drugs in Africa (2). Therefore, new drugs exhibiting distinct mechanism(s) of action that would allow counteracting parasite resistance to drugs in use are urgently needed to sustain and develop treatments against malaria.

In the last decade, we discovered and developed a new potent class of antiplasmodial compounds, the 3-benzylmenadiones (3) with high efficacy against the human erythrocytic stages of *P. falciparum*, in particular against young rings and gametocytes (4). They display no sign of toxicity in host cells or in mice, and have low risk for of glucose-6-phosphate dehydrogenase (G6PD)-deficient populations or populations with hemoglobinopathies (5). The mechanism of action of these redox-cyclers (parent drug or their metabolites) likely involves their bioactivation through a cascade of redox reactions followed by redox-cycling (Scheme 1).



Scheme 1. Proposed mechanisms of action of the antimalarial early-lead plasmidone prodrug (PD) generating toxic metabolites in *P. falciparum*-parasitized red blood cells (pRBC). A first electron (e⁻)

transfer leading to the semiquinone NQH[•] (or a two-e⁻ transfer leading to the dihydro-quinone NQH₂), followed by oxygen insertion at the benzylic position, is proposed to be involved in the drug bioactivation (step 1: bioactivation). This can be catalyzed in enzymatic assays *in vitro* by several relevant pRBC flavoenzymes, including hGR: human glutathione reductase, PfGR: *P. falciparum* glutathione reductase, or PfFNR: *P. falciparum* ferredoxin-NADP⁺ reductase. For the sake of clarity, only the one-e⁻-reduced NQH[•] species was drawn in the developed structures. We previously demonstrated that the second one-electron transfer leading to the dihydronaphthoquinone dianion NQ²⁻ is highly sensitive to the nature of the benzoyl substitution (*p*-CF₃ in **PDO** vs. diverse substituted 3-benzoylmenadiones, see (6)). By generating toxic metabolites, step 2 could lead to parasite killing. In pRBCs, **PD** mimics the effects of mutations in glucose-6-phosphate dehydrogenase (*G6PD*) gene encoding the main producer of NADPH in RBCs (Step 3). Carriers of the most frequent low-activity *G6PD* variants are hematologically normal but present a higher turnover of their RBCs due to oxidative stress and membrane-bound hemichrome in RBCs. It results in phagocytic removal by macrophages and short half-life of RBCs, limiting malaria development.

To understand the mechanism of action of 3-benzylmenadiones, in particular of the most potent antiplasmodial lead plasmodione (**PD**), at the cellular level, we conducted different approaches, including fused-Grx-roGFP-based imaging studies (5,7), physicochemical studies (8-10), genetic screening in yeast (11,12), synthesis of metabolites (5,6,13), chemical tools for proteomics (14), and metabolomics (7). While **PD** affects the redox equilibrium of *P. falciparum*-infected RBCs, its mechanism of action is likely pleiotropic. Each step in the cascade of redox reactions can be catalyzed by different proteins in the different parasitic stages that are sensitive to the compound, supporting the potentially complex behavior of redox-cyclers. In addition, metabolites generated from redox-cyclers are produced in trace amounts, requiring sensitive analytic methods to characterize their mode of action. For instance, using a heavy ¹³C₁₈-isotopically-enriched **PD**, we have recently shown that the apicoplast *P. falciparum* ferredoxin-NADP⁺ reductase (*PfFNR*) was able to generate key drug metabolites (**PD-bzol** and **PDO**) through a 2 h-long redox cycling of **PD** (7). Furthermore, by using the genetically-encoded hGrx1-roGFP2 fluorescent glutathione redox sensor, we could visualize the oxidative stress generated by **PD** in the apicoplast of blood-stage malaria parasites (7). This suggests that a fast pulse of reactive oxygen species (ROS) is released in the apicoplast, possibly mediated by **PD** redox cycling catalyzed by *PfFNR* and/or other apicoplast flavoenzymes. However, many other electron protein acceptors could account for the killing effects of **PD** in the various stages of *P. falciparum*.

The basic six-membered heterocycles, pyridine and pyrimidine, are widely represented in numerous natural products and used in medicinal science (15,16). The replacement of benzyl rings by *N*-heteroaromatics on small organic molecule can have a huge impact on both drug biological activities and physicochemical properties. These last parameters can include the hydrophilicity due to their low basicity especially in acid conditions, the ability to form hydrogen bonds with surrounding molecules due to nitrogen lone pair and the bioisosteric replacement of amine, amide, or benzene rings by the heterocycles (17). A few of aza-analogues of 3-benzylmenadiones have been previously synthesized to examine the effect of nitrogen in the menadione core on redox potentials and inhibitory capabilities (18). **PD** is highly lipophilic, so with this in mind and in order to improve the pharmacokinetic properties of the series, here we report the synthesis and evaluation of the antiplasmodial activity of heteroaromatic analogues of **PD** and various 3-benzylmenadione derivatives (Figure 1).

Moreover, a considerable uncertainty remains about the cellular target(s) of **PD**, that have, so far, been essentially investigated through phylogenetically-distant model organisms like yeast, or by hypothesis-driven targeted experiments in *P. falciparum*. *P. falciparum* can be cultured *in vitro* and manipulated genetically. Still the ring stage is one of the smallest eukaryotic cells known (~1–2 μm), which is a considerable hurdle for microscopic studies and phenotypic

characterization. On the other hand, closely-related apicomplexan parasite *Toxoplasma gondii* is more amenable to cell biology studies because of its larger size and the availability of many cell markers and the relative ease with which the parasite can be studied with various microscopic techniques. *T. gondii* and *P. falciparum* share much of their underlying biology, thus *T. gondii* is also an attractive model to decipher key features related to the Apicomplexa phylum (19). *T. gondii* is responsible for human toxoplasmosis which, although less lethal than malaria, is a major chronic public health problem worldwide: about one third of the human population is infected with this parasite than can cause severe symptoms in immunocompromised individuals (in the context of HIV, leukemia, cancer therapies, or organ transplant) (20). Thus, in parallel, we conducted an initial structure-activity relationship (SAR) study with a reduced number of compounds in *T. gondii* tachyzoites (the stage responsible for the acute phase of the disease) and tracked several **PD**-based probes that allowed us to confirm that **PD** is likely primarily targeting the apicoplast and apicoplast-related functions in Apicomplexa.

Finally, we performed the first ecotoxicity study of our compounds in two model organisms, an algae and a planktonic crustacean. Results of such studies will be key to further inform the MedChem pipeline and improve the safety of novel antiparasitic 3-benzylmenadiones.

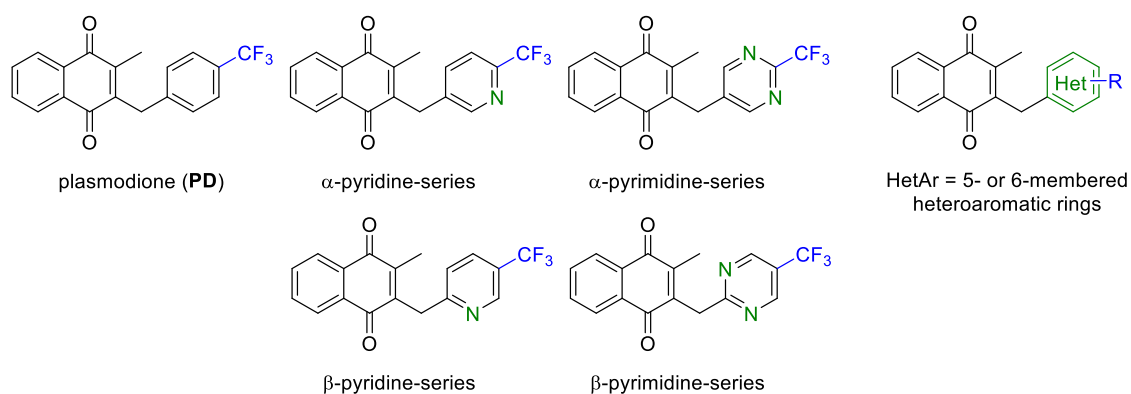
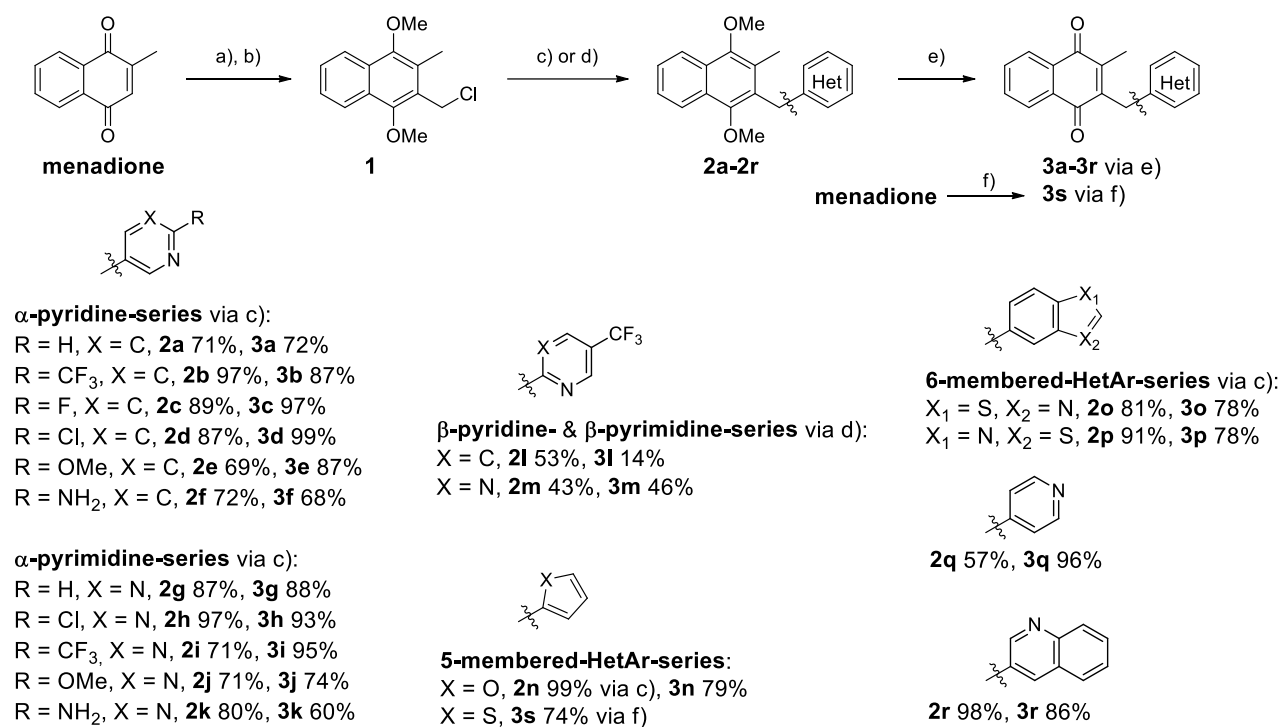


Figure 1. Heteroaromatic analogues of plasmodione and related 3-benzylmenadiones.

■ RESULTS AND DISCUSSION

Synthesis of Heteroaromatic Plasmodione Analogues. The general synthetic route for most of the 3-heterobenzyl-menadione derivatives is presented in Scheme 2. It involved the sequential reduction then protection from the commercially-available menadione and chloromethylation of 1,4-dimethoxy-2-methylnaphthalene (**3**). The resulting chloromethyl derivative **1** was engaged in a Suzuki cross-coupling reaction, using the corresponding boronic acid heteroaryl building blocks. This reaction successfully promoted the formation of the desired product with moderate to excellent yields from 57% for **2q** to 99% for **2n**. Nevertheless, due to incompatibility of the Suzuki cross-coupling reaction with starting α -boron-pyridine and -pyrimidine (even in excess), a Negishi cross-coupling was performed from the corresponding α -halide-pyridine and -pyrimidine, yielding the desired products **3m** and **3l** with moderate yield (21). This incompatibility could be explained by a fast protodeboronation in the Suzuki conditions especially with an N-H, or polarized NC-H group adjacent to the boronate that can stabilize it during C-B fragmentation or an adjacent antibonding orbital (C–N σ^*) that can overlap with the carbanion formally generated during C-B fragmentation (22). Subsequently, the 1,4-quinone moiety was recovered by oxidative demethylation. Only **3s** was obtained in a

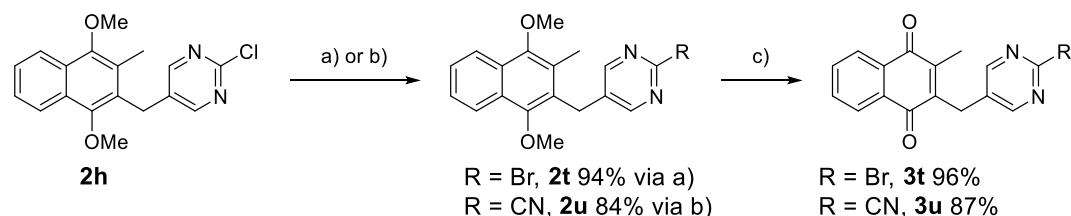
different way from menadione by applying a Kochi-Anderson reaction leading to the desired product in one step.



Reaction conditions: a) 1. SnCl₂, HCl, EtOH, rt, 2 h, 2. Me₂SO₄, acetone, KOH, MeOH, 60°C, 4 h, 93%; b) CH₂O, HCl, 80°C, 2 h, 81%; c) Pd(PPh₃)₄, Na₂CO₃, DME:H₂O, 100°C, 1 h and corresponding boronic acid; d) 1. Mg, LiCl, ZnCl₂, THF, rt, 2 h, 2. Pd(PPh₃)₄, THF, 80°C, 24 h, and corresponding halide; e) CAN, CH₃CN:H₂O, rt, 1 h; f) 2-thiopheneacetic acid, AgNO₃, (NH₄)₂S₂O₈, CH₃CN:H₂O, reflux, 4h.

Scheme 2. Synthesis of heteroaromatic analogues of plasmodione.

Post-modification of α-chloro-pyrimidine **2h** was performed to obtain either the bromo α-pyrimidine after a halogen substitution using TMSBr, or the cyano α-pyrimidine after a nucleophilic aromatic substitution using NaCN. The desired α-pyrimidine **3t** and **3u** were subsequently obtained with good yield after an oxidative demethylation (Scheme 3).

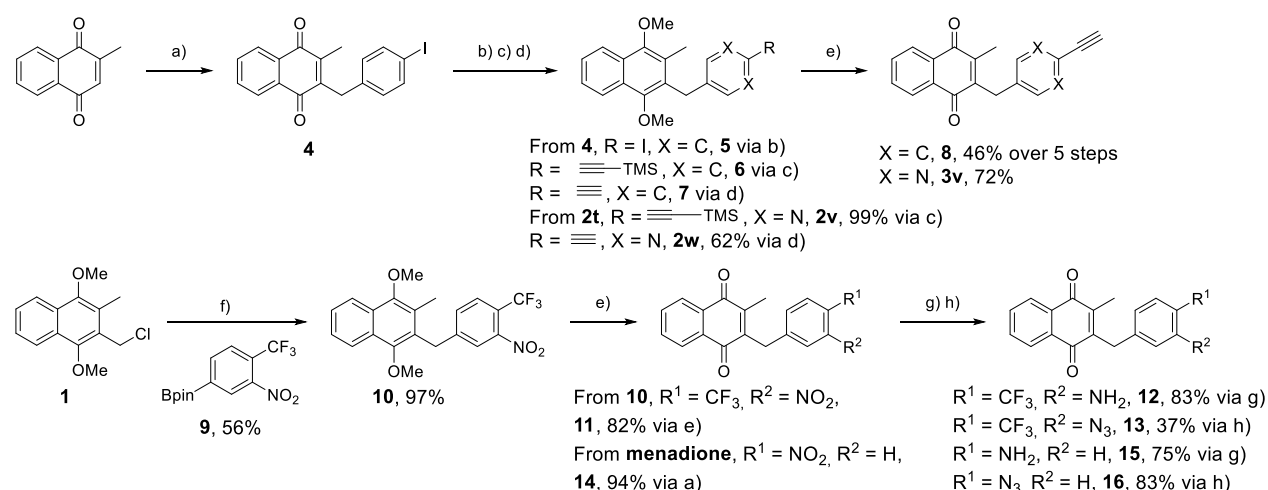


Reaction conditions: a) TMSBr, propionitrile, 100°C, 5 h; b) NaCN, DABCO, DMSO:H₂O, 50°C, 20 h; c) CAN, CH₃CN:H₂O, rt, 1 h.

Scheme 3. Synthetic post-modification to prepare the bromo α-pyrimidine **3t** or the cyano α-pyrimidine **3u**.

Synthesis of clickable plasmodione analogues. The clickable alkyne **8** was synthesized using the reported synthetic route (14) under the compound code **11** with the following slight modifications. The first four steps were launched from crude mixtures without any purification step to isolate the intermediates, enabling a significant gain of time and yield. The single purification was performed after the oxidative demethylation allowing production of the desired product with a 46% overall yield (Scheme 4). Another clickable alkyne **3v**, this time bearing a α -pyrimidine, was obtained with the goal of increasing the aqueous solubility to enhanced the activity. The synthetic route involves a three-steps protocol starting from α -pyrimidine **2t** described above by a Sonogashira cross-coupling reaction with a TMS protected ethynyl, then its deprotection using TBAF followed by the oxidative demethylation (Scheme 4).

Two azido analogues of **PD** were also synthesized to validate its biological target with additional bioimaging results based on a Cu(I)-catalyzed Azide-Alkyne Cycloaddition reaction (CuAAC). Compound **16** was obtained in three steps from menadione by sequential Kochi-Anderson reaction, then a hydrogenation using Pd/C to reduce the nitro group into the amine, followed by a diazotransfer reaction using a water/ionic liquid mixture (1-methyl-2-oxopyrrolidin-1-ium hydrogen sulfate) in a mortar producing the desired azido derivative (**23**) (Scheme 4). Another azido analogue was synthesized with the azide in β position of the para trifluoromethyl group to give the clickable **PD** analogue **13**. The synthetic route starts by a Suzuki cross-coupling from chloromethyl derivative **1** and the Bpin boronic ester **9** obtained by Miyaura borylation. After an oxidative demethylation and finally the same two steps as for **16**, the desired product was obtained with a 12% overall yield (Scheme 4).



Scheme 4. Synthesis of the clickable 3-benzylmenadione alkynes **8**, **3v** and 3-benzylmenadione azides **13**, **16**.

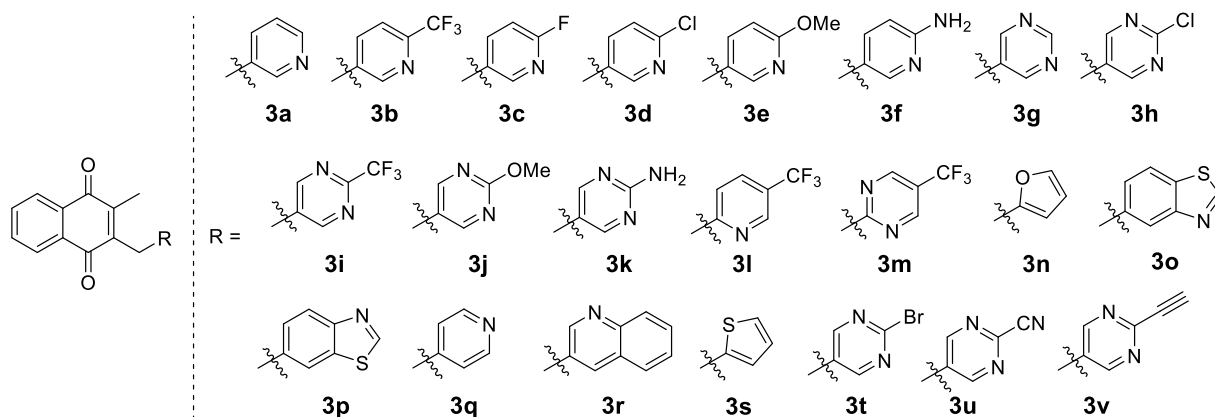
Reaction conditions: a) 4-iodophenylacetic acid or 4-nitrophenylacetic acid, AgNO₃, (NH₄)₂S₂O₈, CH₃CN:H₂O, reflux, 4 h; b) 1. SnCl₂, HCl, EtOH, rt, 2 h, 2. Me₂SO₄ acetone, KOH, MeOH, 60°C, 4 h; c) ethynyltrimethylsilane, CuI, Pd(PPh₃)₂Cl₂, NEt₃, 70°C, 20 h; d) TBAF, THF, rt, 1.5 h; e) CAN, CH₃CN:H₂O, rt, 1 h; f) **9**, Pd(PPh₃)₄, Na₂CO₃, DME:H₂O, 100°C, 1 h; g) 1. Pd/C, EtOH, EtOAc, rt, 16 h, 2. Acetone, rt, 72 h; h) NaNO₂, NaN₃, H₂O:ionic liq., rt, 30 min.

Antimalarial activity of heteroaromatic analogues of plasmodione and related 3-benzylmenadiones

The antimalarial activity of the synthesised **PD** analogues and their related 3-benzylmenadiones was measured against *P. falciparum* strain NF54 using a [³H]-hypoxanthine incorporation assay (24) (Table 1). All compounds displayed submicromolar IC₅₀ activity values

with the exception of the low micromolar activity observed with compounds **3g**, **3r**, and **3v**. The most active compounds **3b**, **3i**, **3t**, **8** (clickable compound) and **13** had IC₅₀ values below 100 nM and thus were comparable to **PD**.

Table 1. Initial SAR study: *In vitro* antiplasmodial and cytotoxicity data expressed as IC₅₀ and CC₅₀ values, respectively, and calculated physicochemical properties.



^a: Values are the mean IC₅₀ value of (2) independent determinations. ^b: IC₅₀ (μM) with the ³H-

Product	Synthetic Process	NF54 IC ₅₀ (μM) ^a	L6 CC ₅₀ (μM)	cLogP	tPSA
3a	Suzuki	0.596	33.5	3.04	46.5
3b	Suzuki	0.065	48.3	4.07	46.5
	Negishi	0.078 ± 0.024	50.9		
3c	Suzuki	0.368	55.1	3.26	46.5
3d	Suzuki	0.496	56.1	3.83	46.5
3e	Suzuki	0.295	53.4	3.86	55.73
3f	Suzuki	0.309	nd	2.71	72.52
3g	Suzuki	1.586	24.8	2.08	58.86
3h	Suzuki	0.251	58.4	2.83	58.86
3i	Suzuki or Negishi	0.194 ± 0.125	179.2	3.03	58.86
3j	Suzuki + post	0.809	86.9	3.03	68.09
3k	Suzuki + post	0.738	Not determined yet	2.07	84.88
3l	Negishi	0.069 ± 0.024	8.82	4.07	46.5
3m	Negishi	0.414 ± 0.293	17.56	3.03	58.86
3n	Suzuki	0.501	4.2	3.71	43.37
3o	Suzuki	0.235	50.29	4.47	46.5
3p	Suzuki	0.37	49.81	4.47	46.5
3q	Suzuki	0.109 ^b	3.12 ^c	3.04	46.5
3r	Suzuki	1.538	136.3	4.42	46.5
3s	Kochi-Anderson	0.427	19.4	4.18	34.14
3t	Suzuki + post	0.041	39.9	2.98	58.86
3u	Suzuki + post	0.816	13.9	1.80	82.65
3v	Suzuki + post	1.648	4.67	2.35	58.86
PD	Kochi-Anderson	0.043 ± 0.002	141.7	5.42	34.14
CQ	-	4.0 ± 0.37 ng/ml			
artesunate	-	2.2 ± 0.66 ng/ml			
Podophyllotoxin	-		0.018-0.010		

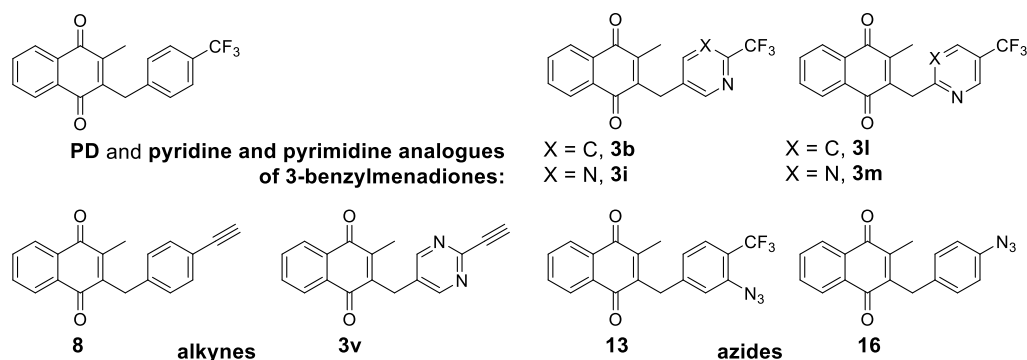
hypoxanthine incorporation-based assay using the *P. falciparum* Dd2 strain, which is sensitive to **PD**,

and resistant to chloroquine (IC_{50} CQ = 0.148 μ M), as reported in (18). ^c: CC_{50} (μ M) using the human MRC-5 cell line, as reported in (18). "post" means post-functionalization.

The β -pyrimidine 3-benzylmenadione analogue 3m is a potent inhibitor of *T. gondii* tachyzoites growth *in vitro*

A set of selected α - and β - pyridines and pyrimidines analogues of **PD** and other 3-benzylmenadiones were tested for their impact on the growth of *T. gondii* tachyzoites by plaque assay (Supporting Information, Figure S1). This assay allows the visualization of the successive lytic cycles of the tachyzoites that generate plaques in the host cell monolayer if parasite fitness is not affected. Atovaquone, a 2-hydroxy-naphthoquinone inhibiting the mitochondrial respiratory chain, and well-known inhibitor of *T. gondii* tachyzoite growth (25), was also included in the analysis. All compounds displayed an effect on parasite growth, with an IC_{50} in the low micromolar range (Table 2, Supporting Information, Figure S2). Although these IC_{50} values were at least 20-fold higher than the one of atovaquone, **PD** and its derivatives remain potent inhibitors of *Toxoplasma* tachyzoites growth *in vitro*.

Table 2. IC_{50} values of plasmodione-derived compounds on *T. gondii* tachyzoites, *P. falciparum*-infected red blood cells, and CC_{50} values to express the cytotoxicity against the rat L6 cell line.



Product	Series	alkyne or Azide	<i>P. falciparum</i> NF54 IC_{50} (μ M) as mean \pm SD	<i>T. gondii</i> IC_{50} (μ M) ^b	L6 CC_{50} (μ M)
3b	α -pyridine	-	0.078 \pm 0.024	5.2 \pm 0.74	50.9
3i	α -pyrimidine	-	0.194 \pm 0.125	8.0 \pm 3.01	179.2
3l	β -pyridine	-	0.069 \pm 0.024	5.7 \pm 0.55	8.82
3m	β -pyrimidine	-	0.414 \pm 0.293	2.1 \pm 0.30	17.56
3v	α -pyrimidine	alkyne	1.648	5.25 \pm 0.43	4.67
8	3-benzylmenadione	alkyne	0.049 \pm 0.015 ^a	9 \pm 1.51	52.30
13		azide	0.0325	nd	63.6
16		azide	0.151	nd	39.65
PD	3-benzylmenadione lead	-	0.043 \pm 0.002	4.0 \pm 1.36	141.7
Artesunate	control	-	0.0057 \pm 0.0017	-	-
Atovaquone	control	-	-	0.102 \pm 0.01	-

^a: IC_{50} (μ M) with the SYBR green assay using the *P. falciparum* Dd2 strain, which is sensitive to PD (20 \pm 5), DHA (IC_{50} DHA = 0.7 \pm 0.2), to methylene blue (IC_{50} MB = 7 \pm 0.3), and resistant to chloroquine (IC_{50} CQ = 189 \pm 12), (14). ^b: IC_{50} values for each compound were calculated based on three independent plaque assays conducted with *T. gondii* tachyzoites as illustrated (Supporting information, Figure S1).

The apicoplast is the primary target of plasmodione and related heteroaromatic 3-benzylmenadiones derivatives in *T. gondii*

As the mode of action of **PD** has been recently linked with enzymatic activities hosted by the mitochondrion in yeast (11,12) and the apicoplast in *Plasmodium* (7), we investigated the impact of the three selected 1,4-naphthoquinones on the morphology of these organelles in *Toxoplasma* by immunofluorescence. To this end, we used the E2 subunit of pyruvate dehydrogenase (PDH-E2) (26) and the F1 beta ATPase (27) as protein markers of the apicoplast and mitochondrion, respectively. We selected **PD** (with an IC₅₀ value of 4 μM), as well as both α-pyrimidine **3i** and β-pyrimidine **3m** (the 1,4-naphthoquinones with the least and the most impact on *T. gondii* growth, with IC₅₀ values of about 8 and 2 μM, respectively) to further study their effect on tachyzoite morphology during the intracellular development of the parasites. For this, intracellular parasites were incubated for three days in the presence of 10 μM of each compound. Immunofluorescence labelling with a marker of the inner membrane complex (a structure made of flattened vesicles underlying the plasma membrane), allowed visualization of developing daughter cells during cell division, which is usually synchronized within each parasitophorous vacuole (Figure 2A). Upon drug treatment, parasite division appeared largely asynchronous within the vacuoles, suggesting that parasite division was affected (Figure 2A). The overall aspect of the mitochondrion, a single organelle with different morphological forms in the parasites (28), was slightly but significantly affected by treatment with the three compounds (Figures 2B and 2C). It will be interesting to investigate whether they also affect mitochondrial metabolism. On the other hand, all three compounds showed a marked impact on the apicoplast, with up to 30% of individual parasites and up to 60% of the parasite-harboring parasitophorous vacuoles displaying a potential loss of the organelle, as assessed by the loss of the PDH-E2 signal (Figures 2B and 2C).

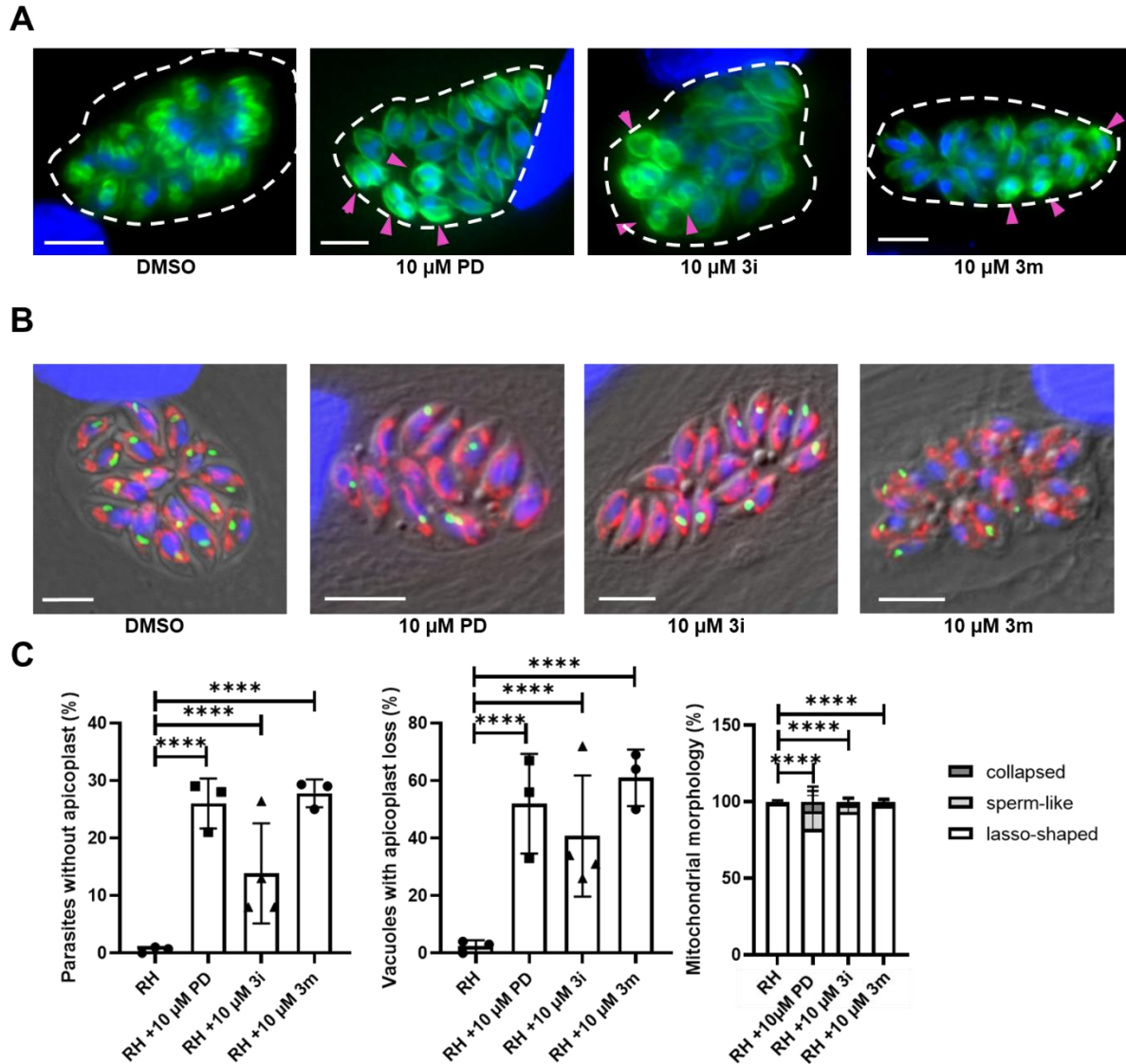


Figure 2. Effect of plasmodione-derived compounds on *T. gondii* parasite division and organelle morphology. A) Treatment with **PD**-derived compounds impacts parasite division. While parasite division is usually synchronized within the same vacuole (outlined with dashed lines), treatment with **PD**, or compounds **3i** and **3m** for 3 days at 10 μ M led to heterogenous vacuoles containing several dividing parasites (arrowheads) together with non-dividing ones as determined by staining with the inner membrane complex marker IMC3 (green). DNA was stained with DAPI (blue). Scale bar represents 10 μ m. B) **PD**-derived compounds impact the homeostasis of the apicoplast. Parasites were treated for three days with each compound and the apicoplast (green) and mitochondrion (red) were stained with specific antibodies. DNA was stained with DAPI (blue). RH is a laboratory-adapted type I *T. gondii* strain. Merged images between fluorescent signals and differential interference contrast are shown. Scale bar=5 μ m. C) Quantification of apicoplast loss *per vacuole* or *per parasite* and of mitochondrial morphology in treated parasites. Percentages for each experiment, and mean \pm SD of at least $n=3$ independent biological replicates are plotted. Differences between treated and untreated parasites were analysed using Fisher's exact test based on the total number of parasites that were counted (parasite counts *per condition* and *per experiment* are summarized in the supporting Information, Tables S1-S3). **** $p \leq 0.0001$.

Lipidomic profile of neosynthesized fatty acids in the apicoplast of *T. gondii* tachyzoites under drug treatment

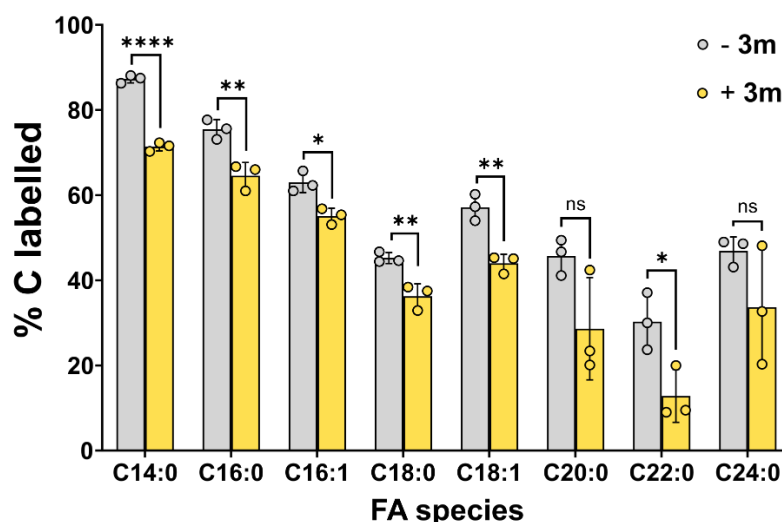
The apicoplast has a central metabolic contribution to the fitness of *T. gondii* tachyzoites. Indeed, the organelle is known to be a major metabolic hub for the parasite (29) notably being the centre for *de novo* synthesis of fatty acids (FA) via its type II prokaryotic Fatty Acid Synthesis pathway (FASII), and of lysophosphatidic acid, a central phospholipid precursor. Both pathways are essential for bulk phospholipid synthesis, membrane biogenesis and thus intracellular parasite survival (30,31). To further determine the impact of the compounds on the apicoplast, and hence its metabolic activity, we investigated whether the FASII pathway was still active upon treatment with the most active β -pyrimidine **3m**. To do so, we used our state-of-the-art approach based on stable isotope labelling combined to mass spectrometry-based lipidomic analysis (32-34). The apicoplast FASII is the only pathway that can use ^{13}C converted from U- ^{13}C -glucose by the parasite glycolysis to PEP that is imported into the apicoplast to generate FA (31,32). Hence, monitoring the ^{13}C incorporation into parasite FA/lipids by GCMS-based lipidomics analyses provides direct evidence on the activity of apicoplast FASII. Briefly parasites treated or not with compound **3m** were grown in human host cells in the presence of U- ^{13}C -glucose (uniformly- ^{13}C labeled glucose). Short times of drug incubation in *T. gondii* tachyzoites were chosen for subsequent ^{13}C incorporation analyses to identify the effects of **3m** on FASII upon using ^{13}C -glucose labelling coupled to GCMS analyses.

In the absence of the drug, the distribution of FA species from C14:0 to C24:0 was found as previously reported (31) upon ^{13}C integration from ^{13}C glucose catabolism. Tachyzoites treated with **3m** for short times, i.e. 4h to retain a fair proportion of organelles, showed significant effects on their global FA synthesis profiles from C14:0 to C24:0 (Figure 3A). Upon drug treatment, the analysis and quantification of FA species according to parasite cell numbers (nanomoles of lipids/parasite/sample), showed an overall decrease in the amount of most major FASII-synthesized FAs (Figure 3A). This reduction in major C14:0, C16:0, C16:1 species would be consistent with a reduced FASII activity, subsequent to the inhibition of an apicoplast protein target resulting in apicoplast loss. To confirm this reduction in apicoplast FASII activity, we carefully analysed ^{13}C incorporation in the isotopomers of C14:0 made by the apicoplast FASII. We confirmed that the *de novo* synthesis of C14:0 FA species in the apicoplast is drastically inhibited upon **3m** treatment of *T. gondii* tachyzoites. This effect is clearly seen from M10 to M14 isotopologues as there is almost no ^{13}C incorporation in the full chain length upon drug treatment. The apparent greater ^{13}C incorporation from M0 to M9 isotopologues may be explained by the fact that *T. gondii* tachyzoites grow in host cell types that can potentially provide them with more FA resources. Of note, the nutrient-rich *in vitro* culture systems also mask some important contributions to scavenge exogenous metabolites as precursors of FA, as previously documented (31,35). The distribution of ^{13}C incorporation in the isotopomers of C16:0 and C16:1 follows the same pattern upon drug treatment (see Supporting information, Figures S3 to S10). Concerning the elongated species synthesized in the endoplasmic reticulum from C18:0, C18:1 to C20:0, C22:0, C24:0, there is almost no ^{13}C incorporation in the full chain length in the presence of β -pyrimidine **3m**.

Taken together, these lipidomics analyses thus confirm that the apicoplast FASII activity is compromised by the treatment, likely due to an early disruption of the global homeostasis of the apicoplast.

A

Carbon integration Glucose-13C



B

Abundance average - C14:0

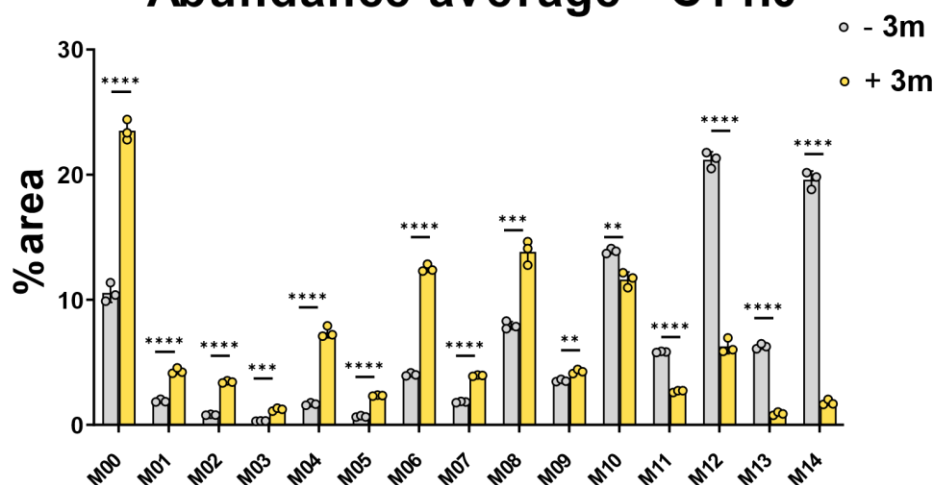


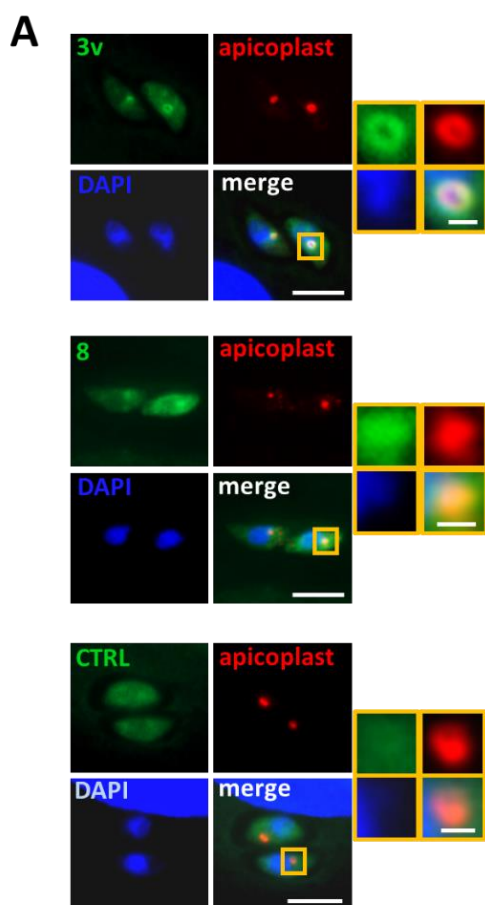
Figure 3. A) Effect of the PD-derived compound **3m** on the de novo synthesis of fatty acids via the apicoplast FASII based on U-¹³C-glucose labelling coupled to GCMS analyses in *T. gondii* tachyzoites. Incorporation of ¹³C from the apicoplast FASII is significantly reduced in all parasite FA species. B) ¹³C incorporation analysis in the isotopomers of C14:0 made by the apicoplast FASII. De novo synthesis of C14:0 fatty acids in the apicoplast is drastically inhibited upon compound **3m** treatment of *T. gondii* tachyzoites, as there is almost no ¹³C incorporation in the full chain length.

Values, mean ± SEM of 3 independent replicates were plotted. Differences between treated (yellow) and untreated (gray) parasites were analysed by a t-test for each lipidomic analysis (GraphPad Prism 10): ns, non-significant; *, p<0.05; **, p<0.01; ***, p<0.001; ****, p<0.0001.

Drug localization studies in *T. gondii* tachyzoites

To gain further insights into a specific impact of the compounds on the apicoplast in *T. gondii*, we used the clickable compounds **3v** and **8** to perform localisation experiments. These alkyne derivatives were found to have similar IC₅₀ on the growth of *T. gondii* tachyzoites as the 3-benzylmenadione they derived from (Table 2). Microscopy analysis of fluorescent dye-conjugated compounds and co-staining with an apicoplast-resident protein showed an

accumulation of compounds **3v** and **8** in the organelle after 6 hours of incubation (Figure 4A). This was in sharp contrast to the control condition in which the click reaction was performed with the fluorescent azide without prior incubation with the compounds, and for which fluorescent labelling was distributed homogenously in the cytosol (Figure 4A). The enrichment of the compounds at the apicoplast was further confirmed by analysing the distribution of the fluorescence signal in the parasites (Figure 4B). Apicoplast labelling was consistently observed in the majority of *Toxoplasma* tachyzoites: $85 \pm 8\%$ with compound **3v** and $75 \pm 3\%$ with compound **8** ($n=3$ independent experiments, an average of 50 parasites were counted for each condition). Altogether, these data strongly suggest that 3-benzylmenadiones act on *T. gondii* by targeting primarily the apicoplast and have a marked effect on the organelle that is likely contributing to their impact on parasite growth.



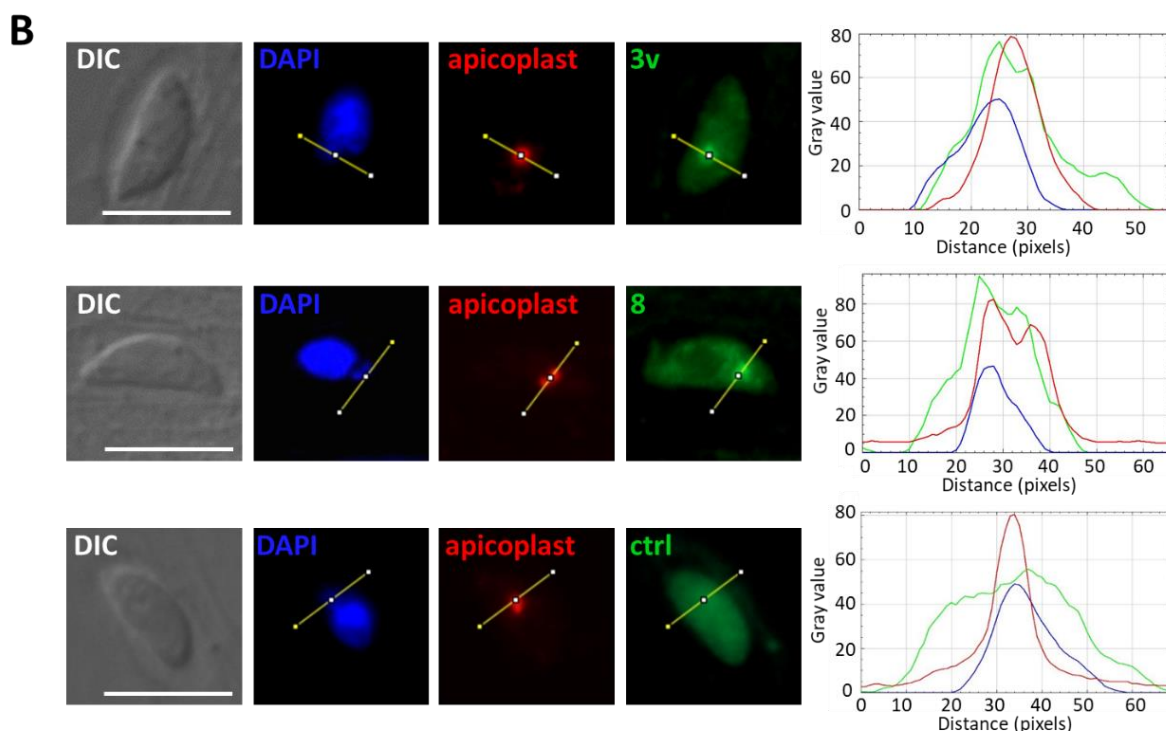


Figure 4. A) **3v** and **8** were incubated for 6 hours with intracellular tachyzoites and were labelled with a fluorescent azide by click chemistry (green) before co-staining with the anti-PDH-E2 antibody to label the apicoplast (red). DNA was stained with DAPI (blue). Magnified insets show the vicinity of the apicoplast to highlight colocalization. In the control (bottom), the click reaction with the fluorescent azide was performed without pre-incubation with a **PD**-derived compound. Scale bar represents 5 μm (large field) or 0.5 μm (inset). B) Fluorescence intensity profiles show the distribution of fluorescence across the orange line (x-axis). The fluorescence intensities are plotted along the y-axis and highlight the close proximity of the peaks for apicoplast-localized DNA (in blue, the apicoplast has its own genome), apicoplast-resident protein PDH-E2 (in red) and **PD**-derived compound (in green). DIC: differential interference contrast. Scale bar represents 5 μm .

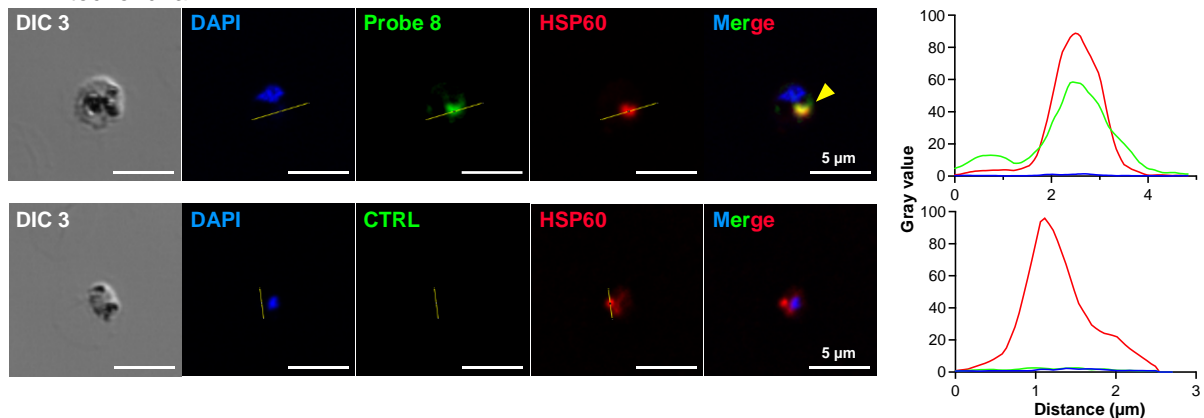
A localization experiment was also performed on azido **PD** analogues **13** and **16**. However, no fluorescence signal could be observed after 6 h of incubation and the click reaction using the commercial Alexa Fluor 488 alkyne. This may be explained by the fact that aryl azides are known to be unstable under the click reaction conditions (i.e. the presence of biological reductant or UV irradiation), although in our case we validated their stability *in vitro* (Supporting information, Figures S11-S13, NMR spectra of the azido derivative **16** incubated for 24 h under excess of sodium ascorbate, GSH, or cysteine).

Drug localization in *P. falciparum* trophozoites

We further used two clickable probes, namely probes **3v** and **8**, on trophozoites of *P. falciparum* NF54 strain. Young trophozoite parasites were treated with the probes for 2 and 4 h to assess their distribution and potential colocalization with specific organelles such as the mitochondria or apicoplast. The results revealed distinct patterns for the two probes. Probe **3v** exhibited a homogeneous distribution within the parasite, with no noticeable accumulation (see Supporting information, Figure S14). In contrast, probe **8** distribution was heterogenous and usually accumulated close to, or colocalized with, the mitochondrion or apicoplast (Figure 5

and Supporting information, Figure S15). We observed an association of probe **8** with the mitochondria or apicoplast signals in 27-30% and 19-24% of the parasites, respectively (n=2 independent experiments, an average of 140 parasites were counted for each condition, Supporting information, Table S4). Of note, the fact that probe **8** signal appeared punctuated even when not associating with the labelled organelle (Figure S15) suggests that it accumulated in other organelles, including possibly mitochondria when the apicoplast was labelled, and reciprocally. It will be interesting to investigate whether this colocalization varies with exposure time, parasite stage or drug concentration. Of note, probe **3v** demonstrated lower antiplasmodial activity compared to probe **8**, which raises the possibility of a correlation between the probe activity and its specific accumulation in organelles within the parasite.

A. Mitochondria



B. Apicoplast

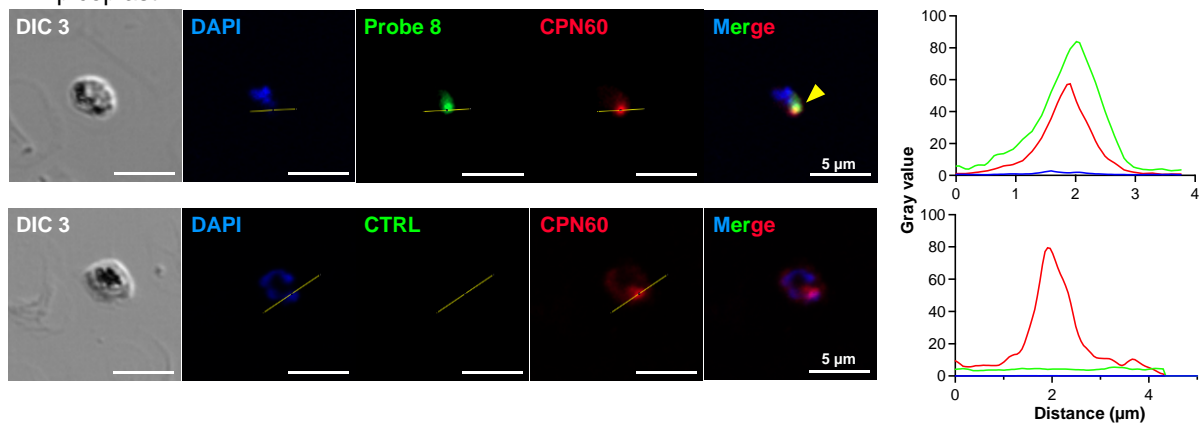


Figure 5. Subcellular localization of probe **8** in asexual blood stages of *P. falciparum* (trophozoite stage) after 2h of incubation. The probe was detected using CuAAC reaction with Alexa Fluor 488-azide (green). Nucleic acids were DAPI-stained (blue), and antibodies specific to *P. falciparum* HSP60 and CPN60 were used to localize the mitochondria (panel A, red) and apicoplast (panel B, red), respectively. Colocalization of probe **8** and the organelle is indicated by yellow arrowheads. Fluorescence intensity profiles were plotted as graphs along the yellow line (x-axis). In control experiments, the click reaction with the fluorescent azide was performed without pre-incubation of parasites with probe **8**. Representative images from 2 biological replicates.

As in *T. gondii*, exposure of *P. falciparum* parasites to **PD** or probe **8**, in this case at 50 nM, i.e., at their IC_{50} and for 14 h and 48 h, led to a strong reduction or complete disappearance of the mitochondria and/or apicoplast signal in 3-12% of all parasites, indicating that these organelles are lost (Figure 6). Of note, the percentage of parasites devoid of apicoplast

increased at cycle n+1 (48 h) as compared to 14 h, which is usually observed when the apicoplast is targeted. The fact that probe **8** is enriched in mitochondria and apicoplast, and that these two organelles are lost in some parasites upon treatment, suggest that parasite killing upon 3-benzylmenadione treatment may be mediated by an effect of the drug on the apicoplast and/or mitochondria, although we cannot exclude that the loss of apicoplast and/or mitochondria could be a consequence, rather than the cause, of parasite death (Figure 6).

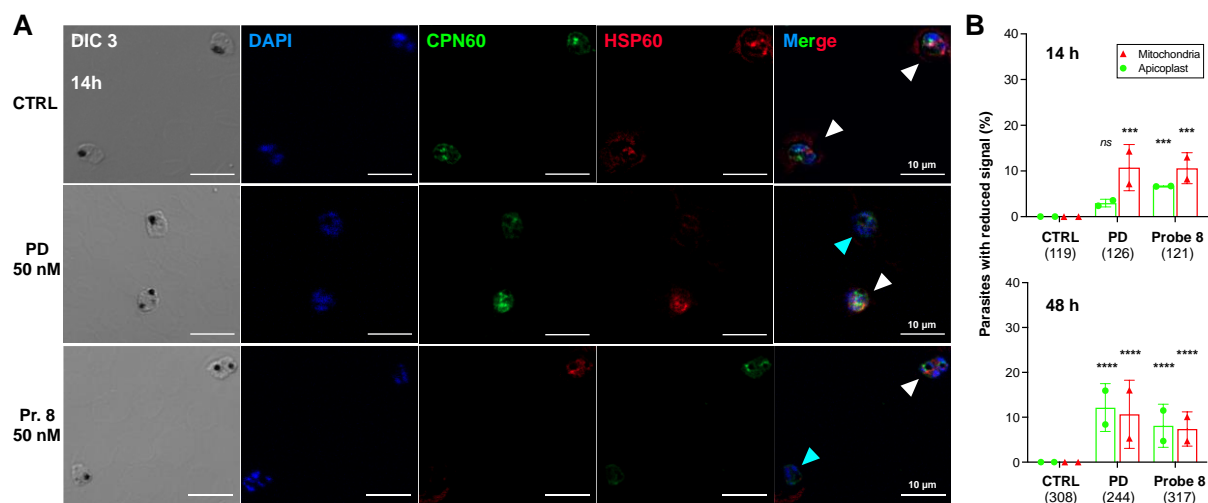


Figure 6. Morphological analysis of *P. falciparum* parasites after exposure to **PD** or probe **8** at 50 nM. A) Subcellular localization of apicoplast (CPN60, green), mitochondria (HSP60, red) and nucleic acids (DAPI, blue) in asexual blood stages of *P. falciparum* (trophozoite stage) after 14 h of treatment and in untreated parasites (CTRL). Parasites presenting normal apicoplast and mitochondria signal are indicated with white arrowheads, those presenting reduced/no signal for both markers are indicated with cyan arrowheads. Representative images from 2 independent experiments. B) Quantification of apicoplast and mitochondrial loss in parasites after 14 h and 48 h of exposure to **PD** or probe **8** at 50 nM. Data from the same experiments as A. Percentages for each experiment and mean \pm SD are plotted. Differences between treated and untreated parasites were analyzed using Fisher's exact test based on the total number of parasites that were counted (indicated in brackets below each condition; parasite counts *per* condition and *per* experiment are summarized in the Supporting Information, Table S4). *ns*, non-significant; ***, $p < 0.005$; ****, $p < 0.0001$.

Discussion on the structure-activity relationships

The main conclusions on the structure/activity relationships tested in this study are summarised in Table 3, including anti-Apicomplexa activities based on IC_{50} values, imaging of morphological alterations, drug localization by the CuAAC reaction and lipidomics analyses.

Our results demonstrate that the apicoplast is a major target of 3-benzylmenadiones in *T. gondii*. Indeed, treatment of *T. gondii* tachyzoites with three compounds, **3m**, **3i** and **PD**, led to alterations in the apicoplast (i.e. a reduction of the number of parasites carrying an apicoplast). These alterations were more severe upon treatment with **3m** and **PD** that are more potent on *T. gondii* tachyzoites, than with **3i** presenting a higher IC_{50} value. Lipidomics analyses confirmed that the FASII pathway, located in the apicoplast was strongly affected by **3m** treatment. Finally, using two clickable probes with different potencies, **3v** and **8**, we also

demonstrate that the 3-benzylmenadiones localise in the apicoplast, with a correlation between potency and concentration of the probe.

In *P. falciparum*, the ‘clickable’ benzylmenadione-alkyne probe **8** exhibited similar IC₅₀ values as the lead **PD** (IC₅₀ ca. 45 nM) whereas probe **3v** was less potent (IC₅₀ > 2 μM). Both compounds were found to accumulate in the parasites by CuAAC-based imaging. Still, their distribution was different: probe **3v** was homogeneously distributed in the parasite while probe **8** showed subcellular accumulations that colocalised with the apicoplast and mitochondria in 20-30% of the cases. The differences in probe distribution and colocalization patterns may reflect variations in their potency, mechanism of action or affinity for specific targets.

Table 3. Structure-activity relationships.

Structure-Activity relationships	<i>T. gondii</i> tachyzoites	<i>P. falciparum</i> trophozoites
Activity (based on IC ₅₀): + → -	3m > PD > 3b = 3v > 3l > 3i = 8	PD = 8 > 3l > 3b > 3i > 3m > 3v
Morphological alterations	3m > PD > 3i (apicoplast disrupted)	nd
Drug localization by click	3v > 8 (in apicoplast)	8 > 3v (in apicoplast & mitochondria)
Lipidomics	3m (apicoplast FASII lipids affected)	nd

Discussion on the possible mode of action of 3-benzylmenadiones

The loss of the apicoplast is often associated with the delayed death of the parasite, which is usually the case for most housekeeping pathways and processes held in the apicoplast, such as organellar genome replication/transcription/translation. Hence, most apicoplast inhibitors that are directed against prokaryotic-like pathways of the apicoplast, such as clindamycin, doxycycline or azithromycin, induce a delayed death of the parasite (36-38). It is also the case for some inhibitors affecting non-housekeeping processes, such as single metabolic pathways of the apicoplast (i.e., fatty acid synthesis, isoprenoid synthesis, heme and iron-sulfur cluster, see refs 29 and 39). This phenomenon was partially explained by the loss of the apicoplast causing the slow arrest of protein prenylation in subsequent parasite generation (37). Indeed, the abrogation of several apicoplast pathways at the same time, and/or disruption of the import of major metabolic precursors in the apicoplast can lead to immediate death instead (40). Therefore, it is actually difficult to characterize apicoplast disruption only based on the detection of delayed death. Taken together, our IFAs, and lipidomics/fluxomics data suggest that at least one of the relevant **PD** targets is in the apicoplast. Of note, in *P. falciparum*, the partial association of the ‘clickable’ 3-benzylmenadione **8** (this study) and of a ‘clickable’ 6-fluoro-3-benzylmenadione probe (41), both potent antimalarial compounds, with the apicoplast and mitochondria, is coherent with previous data we obtained in both yeast (mitochondria only) and *P. falciparum*, as detailed below.

First, we previously demonstrated that **PD** inhibits yeast respiratory growth and that the mitochondrial respiratory chain flavoprotein NADH-dehydrogenases play a key role in **PD** activity, and **PDO** redox-cycling (11). Indeed, the deletion of the NDE1 gene encoding the main NADH dehydrogenase in yeast resulted in a decreased sensitivity to **PD** (11). It will be worth investigating whether the homologous parasite protein *P*N_{DH2} is also involved in **PD** mode of action in *P. falciparum*.

Second, and regarding the role of the apicoplast in the mode of action of **PD**, our observations are also in agreement with recent data published by Cichocki *et al.* (7). Using the genetically-

encoded redox sensor hGrx1-roGFP2 expressed in different subcellular compartments of transgenic *P. falciparum* parasites, an oxidative burst was detected in the apicoplast 5 min after **PD** treatment (7), while oxidative stress only peaked 4 h after drug exposure in the cytosol (5). The fact that **PD** influences the apicoplast redox potential more rapidly than the cytosolic one suggests that **PD** bioactivation may occur in the apicoplast. This could be mediated by **PD** redox cycling catalyzed by an apicoplast flavoenzyme such as *P. falciparum* ferredoxin-NADP⁺ reductase (*PfFNR*). Indeed, this enzyme can catalyze single-electron reduction of quinones (42) accompanied by high redox cycling and O₂^{•-} formation, which would be coherent with the early oxidative burst observed in the apicoplast. We also previously demonstrated that the efficient *PfFNR*-catalyzed **PD** bioactivation produced both **PD** key metabolites, **PD-bzol** and **PDO** (7). Finally, we have recently identified several potential **PD** targets in yeast and *P. falciparum* using an affinity-based proteome profiling strategy with a photoreactive and 'clickable' 6-fluoro benzylmenadione probe (41). For instance, of the 11 proteins identified in yeast, 3 are involved in oxidoreductase activities (*Pdb1*, *Dot5*, *Scs7*) and one belongs to the yeast flavoproteome (*Pdx3*). Interestingly, *Pdb1* is the E1 beta subunit of the PDH complex, localized in the mitochondria in yeast, but its orthologous surrogate is found in the apicoplast of *Plasmodium* parasites. In addition to E1, PDH is formed of E2 (dihydrolipoamide acetyltransferase) and E3 (dihydrolipoamide dehydrogenase) components, with the structural protein *Pdx1*. We previously found that E3 (or *Lpd1*) and *Lip2*, acting in the attachment of lipoic acid groups to E2 are involved in **PD** activity (12). Hence, the role of *PfPDH* in **PD** bioactivation will be worth investigating.

In conclusion, the data produced here and in our previous reports provide several lines of evidence pointing towards a mode of action of **PD** and analogues targeting both the parasite apicoplast and mitochondria, with the bioactivation of **PD** into potent metabolites possibly occurring in the apicoplast. Further genetic and functional validations are required to confirm this model.

Ecotoxicity

The second objective of this work aimed at investigating the overall environmental impact of our compounds.

In a first preliminary study based on a selection of three 3-benzylmenadione representatives and heteroaromatic analogues, **PD**, **3b** and **3i** (see structures in Table 2) exhibited heterogeneous toxicities towards algae and invertebrates, as indicated by the calculated EC₁₀, EC₂₀, and EC₅₀-values. After being exposed for 96 h to increasing concentrations of the drugs, the algae *Desmodesmus subspicatus* was affected strongly by **PD**, followed by α -pyridine **3b** and α -pyrimidine **3i**, and all values were in the sub-micromolar range. Of note, *Desmodesmus* is a plastid-bearing green algae, and given the potential link between the mode of action of **PD**-derivatives and the apicomplexan plastid, it might be interesting to further investigate whether these compounds may have a more general impact on plastid-bearing organisms. Planktonic crustacean *Daphnia magna*, was generally less affected, and the compounds with the strongest effect were **3b**, followed by **3i** and **PD** (Table 4). While the number of tested species is quite limited, these data suggest that primary producers are significantly more sensitive than primary consumers. These results call for an extended ecotoxicity analysis with more test species and a particular attention directed to primary producers potentially driving the environmental risk of these compounds. While environmental concentrations have not been estimated during this study, the ecotoxicological data point to **PD** having the highest environmental risks followed by **3b** and **3i**. This information can, under the umbrella of the One

Health Concept, guide the drug development by actively selecting for the most efficient but still environmentally least risky molecules.

These data will enter a database to build a sharable guideline-like document useful for drug designer and managers of environmental risks. Drug ecotoxicity is an emerging environmental problem, and one that is attracting increasing attention from colleagues dealing with pharmaceutical use/manufacturing. Therefore, optimization of 3-benzylmenadiones, headed by **PD**, will progress in a more sustainable approach following the principles of an optimal activity and safety profile in humans, animals and other organisms found in the environment.

Table 4. EC-values (\pm 95% confidence interval) derived from the toxicity tests. Concentrations are given in μ M. n.d. = not determined, as response did not reach the effect level.

Test item	Test organism	EC ₁₀	EC ₂₀	EC ₅₀
PD	<i>Desmodesmus subspicatus</i>	0.015 \pm 0.013	0.214 \pm 0.062	0.556 \pm 0.081
	<i>Daphnia magna</i>	169.45 \pm 63.57	222.71 \pm 59.02	336.52 \pm 44.55
3b	<i>Desmodesmus subspicatus</i>	0.28 \pm 0.12	0.70 \pm 0.15	n.d.
	<i>Daphnia magna</i>	1.77 \pm 0.32	2.28 \pm 0.26	3.34 \pm 0.16
3i	<i>Desmodesmus subspicatus</i>	n.d.	n.d.	n.d.
	<i>Daphnia magna</i>	1.89 \pm 2.39	6.09 \pm 4.03	n.d.

Conclusion

Our study takes advantage of the synthesis of chemical derivatives of **PD** and the use of two related parasite models to investigate the mode of action of this lead compound. Our results highlighted some differences. First, **PD** derivatives were less active in *T. gondii* (low micromolar range) as in *P. falciparum* blood stages (nanomolar range). This could be explained by the presence of new permeability pathways in *Plasmodium*-infected erythrocytes. Indeed, this parasite modifies extensively the host cell membrane that becomes highly permeable to various types of solutes, facilitating the uptake of small compounds, including drugs (43). To reach *T. gondii*, on the other hand, drugs have to cross a series of non-permeable membranes (i. e., the host plasma membrane, the parasitophorous vacuole membrane, the parasite plasma membrane). Thus, **PD**-derived compounds may have to be optimized for their ability to cross membranes if they need to be used in the context of toxoplasmosis.

Another noticeable difference is that, while **PD**-derivatives accumulated in *T. gondii* apicoplast, and treatment with **PD** and analogues clearly affected the morphology and function of the organelle, clickable probe **8** did show a heterogenous localization in *P. falciparum*, but less clearly associated with the apicoplast. Indeed, it showed association with the mitochondrion or the apicoplast in 20-30% of parasites only. Of note, this association with apicoplast and mitochondrion is coherent with studies on the mechanism of action of **PD** in *P. falciparum* (7), and in yeast (11), that proposed both apicoplast- and mitochondrion-based oxidoreductases as potential activators of the pro-drug and redox-cyclers. The differences between the two apicomplexan models do not rule out a conservation of end targets between them, and the converging evidence pointing to a conserved involvement of the apicoplast remains to be investigated further.

■ METHODS

Chemistry. General. All the reagents and solvents were purchased from commercial sources and used as received, unless otherwise stated. The ^1H , ^{19}F and, and ^{13}C $\{^1\text{H}\}$ NMR spectra were obtained in CDCl_3 or DMSO-d_6 as solvents using a 400 MHz or a 500 MHz spectrometer. Chemical shifts were reported in parts *per million* (δ). ^1H NMR data were reported as follows: chemical shift (δ ppm) (multiplicity, coupling constant (Hz), and integration). Multiplicities are reported as follows: s = singlet, d = doublet, t = triplet, q = quartet, m = multiplet, or combinations thereof. High-resolution mass spectroscopy (HRMS) spectra were recorded using the electron spray ionization (ESI) technique.

Synthesis of precursors. Heteroarylboronic acids and reactants were purchased from commercial sources, such as Fluorochem, Sigma-Aldrich, BLDpharm and Alfa Aesar. 1,4-dimethoxy-2-methylnaphthalene was synthesized according to a previously published method (3).

2-(4-iodobenzyl)-3-methylnaphthalene-1,4-dione (4). Synthesized according to a previously published method (13) from menadione but without any purification, the crude mixture was directly engaged in the next step.

2-(4-iodobenzyl)-1,4-dimethoxy-3-methylnaphthalene (5). Synthesized according to a previously published method (14) from **4** but without any purification, the crude mixture was directly engaged in the next step.

((4-((1,4-dimethoxy-3-methylnaphthalen-2-yl)methyl)phenyl)ethynyl)trimethylsilane (6). Synthesized according to a previously published method (14) from **5** but without any purification, the crude mixture was directly engaged in the next step.

2-(4-ethynylbenzyl)-1,4-dimethoxy-3-methylnaphthalene (7). Synthesized according to a previously published method (14) from **6** but without any purification, the crude mixture was directly engaged in the next step.

2-(chloromethyl)-1,4-dimethoxy-3-methylnaphthalene (1). 1,4-dimethoxy-2-methylnaphthalene (1 equiv., 4 g, 19.8 mmol), paraformaldehyde (5 equiv., 3.13 g, 98.9 mmol) and 37% aqueous hydrochloric acid (50 mL) were heated at 80 °C during 2 h. The mixture was cooled down, diluted with water and extracted three times with ethyl acetate. The reunited organic layers were washed with brine, dried over magnesium sulfate, filtered and the solvent was removed under reduced pressure. The crude oil was purified by silica gel chromatography (CHX/T, 8/2, v/v, UV) to afford 2-(chloromethyl)-1,4-dimethoxy-3-methylnaphthalene (4.08 g, 81%) as a colorless oil which crystallized on standing. ^1H NMR (400 MHz, CDCl_3) δ 8.08 (dd, $J = 7.6, 1.8$ Hz, 2H), 7.58 – 7.41 (m, 2H), 4.92 (s, 2H), 4.04 (s, 3H), 3.89 (s, 3H), 2.53 (s, 3H).

General procedure for the Suzuki coupling between 2-(chloromethyl)-1,4-dimethoxy-3-methylnaphthalene and aryl or heteroarylboronic species.

General conditions are a modification of a previously published procedure (44). In a sealable tube, 2-(chloromethyl)-1,4-dimethoxy-3-methylnaphthalene **1** (1 equiv.), the desired heteroarylboronic acid (1.2 equiv.) and sodium carbonate (2.1 equiv.) were dissolved in a 2:1 mixture of dimethoxyethane:water (0.15 M). The mixture was bubbled 30min with argon, and then tetrakis(triphenylphosphine)palladium (2-5 mol%) was added at once. The tube was sealed and the mixture was heated 1 h at 100 °C under stirring. The mixture was then, allowed to cool down to room temperature, diluted with water and extracted three times with ethyl acetate. Reunited organic layers were washed with brine, dried over magnesium sulfate,

filtered and the solvent was removed under reduced pressure to afford a crude which was purified on silica gel chromatography using the adequate eluant system to afford the desired coupling product.

3-((1,4-dimethoxy-3-methylnaphthalen-2-yl)methyl)pyridine (2a). 5 mol% Pd(PPh₃)₄, Eluant (CHX/EtOAc, 5/5, v/v, UV), yellowish solid, 71% yield. m.p. 105-106 °C. ¹H NMR (500 MHz, CDCl₃) δ 8.50 (dd, *J* = 2.3, 1.0 Hz, 1H), 8.41 (dd, *J* = 4.8, 1.6 Hz, 1H), 8.12 – 8.04 (m, 2H), 7.63 – 7.42 (m, 2H), 7.39 – 7.32 (m, 1H), 7.13 (ddd, *J* = 7.8, 4.8, 0.9 Hz, 1H), 4.25 (s, 2H), 3.86 (s, 3H), 3.85 (s, 3H), 2.26 (s, 3H). ¹³C {¹H} NMR (126 MHz, CDCl₃) δ 150.75, 150.73, 149.9, 147.5, 136.1, 135.7, 128.3, 128.0, 127.3, 126.6, 126.1, 125.8, 123.5, 122.6, 122.4, 62.4, 61.6, 30.3, 12.8. HRMS (ESI) calcd. for C₁₉H₂₀NO₂: 294.1489. Found: 294.1490 (M+H⁺).

5-((1,4-dimethoxy-3-methylnaphthalen-2-yl)methyl)-2-(trifluoromethyl)pyridine (2b). 5 mol% Pd(PPh₃)₄, Eluant (CHX/EtOAc, 9/1, v/v, UV), translucent oil, 97% yield. ¹H NMR (500 MHz, CDCl₃) δ 8.64 (d, *J* = 1.4 Hz, 1H), 8.16 – 8.04 (m, 2H), 7.61 – 7.46 (m, 4H), 4.31 (s, 2H), 3.87 (s, 3H), 3.86 (s, 3H), 2.26 (s, 3H). ¹³C {¹H} NMR (101 MHz, CDCl₃) δ 150.82, 150.81, 150.1, 145.9 (q, *J* = 34.6 Hz), 139.7, 136.8, 128.4, 127.2, 127.0, 126.3, 126.2, 125.9, 122.5, 121.8 (q, *J* = 273.7 Hz), 120.3 (q, *J* = 2.7 Hz), 62.3, 61.5, 30.1, 12.8. ¹⁹F NMR {¹H} (471 MHz, CDCl₃) δ -67.68. HRMS (ESI) calcd. for C₂₀H₁₉F₃NO₂: 362.1362. Found: 362.1368 (M+H⁺).

5-((1,4-dimethoxy-3-methylnaphthalen-2-yl)methyl)-2-fluoropyridine (2c). 2 mol% Pd(PPh₃)₄, Eluant (CHX/EtOAc, 9/1, v/v, UV), white solid, 89% yield. m.p. 120-121 °C. ¹H NMR (400 MHz, CDCl₃) δ 7.94 – 7.70 (m, 3H), 7.40 – 7.19 (m, 3H), 6.54 (ddd, *J* = 8.4, 3.1, 0.6 Hz, 1H), 3.98 (s, 1H), 3.63 (s, 3H), 3.61 (s, 3H), 2.03 (s, 3H). ¹³C {¹H} NMR (101 MHz, CDCl₃) δ 162.4 (d, *J* = 237.2 Hz), 150.8, 150.6, 146.9 (d, *J* = 14.4 Hz), 141.0 (d, *J* = 7.6 Hz), 133.6 (d, *J* = 4.5 Hz), 128.3, 127.9, 127.3, 126.4, 126.2, 125.8, 122.6, 122.5, 109.3 (d, *J* = 37.4 Hz), 62.4, 61.6, 29.4 (d, *J* = 1.5 Hz), 12.8. ¹⁹F NMR {¹H} (377 MHz, CDCl₃) δ -72.09 (d, *J* = 8.0 Hz). HRMS (ESI) calcd. for C₁₉H₁₉FNO₂: 312.1394. Found: 312.1403 (M+H⁺).

2-chloro-5-((1,4-dimethoxy-3-methylnaphthalen-2-yl)methyl)pyridine (2d). 5 mol% Pd(PPh₃)₄, Eluant (CHX/EtOAc, 9/1, v/v, UV), white solid, 87% yield. m.p. 123-124 °C. ¹H NMR (400 MHz, CDCl₃) δ 8.19 (dd, *J* = 2.6, 0.8 Hz, 1H), 8.07 – 7.91 (m, 2H), 7.51 – 7.38 (m, 2H), 7.26 (dd, *J* = 8.2, 2.5 Hz, 1H), 7.08 (dd, *J* = 8.2, 0.7 Hz, 1H), 4.13 (s, 2H), 3.78 (s, 3H), 3.77 (s, 3H), 2.18 (s, 3H). ¹³C {¹H} NMR (101 MHz, CDCl₃) δ 150.8, 150.7, 149.5, 149.2, 138.7, 135.1, 128.4, 127.6, 127.3, 126.37, 126.33, 125.9, 124.2, 122.6, 122.5, 62.5, 61.6, 29.6, 12.8. HRMS (ESI) calcd. for C₁₉H₁₉ClNO₂: 328.1099. Found: 328.1102 (M+H⁺).

5-((1,4-dimethoxy-3-methylnaphthalen-2-yl)methyl)-2-methoxypyridine (2e). 2 mol% Pd(PPh₃)₄, Eluant (CHX/EtOAc, 95/05, v/v, UV), translucent oil, 69% yield. ¹H NMR (400 MHz, CDCl₃) δ 8.14 – 8.04 (m, 2H), 8.02 – 7.94 (m, 1H), 7.58 – 7.44 (m, 2H), 7.32 (dd, *J* = 8.5, 2.6 Hz, 1H), 6.61 (dd, *J* = 8.6, 0.7 Hz, 1H), 4.16 (s, 2H), 3.89 (s, 3H), 3.85 (s, 3H), 3.85 (s, 3H), 2.28 (s, 3H). ¹³C {¹H} NMR (101 MHz, CDCl₃) δ 162.8, 150.68, 150.65, 146.0, 138.9, 128.7, 128.6, 128.2, 127.3, 126.7, 125.9, 125.7, 122.6, 122.4, 110.7, 62.4, 61.5, 53.4, 29.4, 12.7. HRMS (ESI) calcd. for C₂₀H₂₂NO₃: 324.1594. Found: 324.1617 (M+H⁺).

5-[(1,4-dimethoxy-3-methylnaphthalen-2-yl)methyl]pyridin-2-amine (2f). 7 mol% Pd(PPh₃), Eluant (EtOAc, 10, v/v, UV), orange solid, 72% yield. m.p. = 95-97 °C. ¹H NMR (400 MHz, CDCl₃) δ 8.08 (tdd, *J* = 5.3, 4.0, 3.2 Hz, 2H), 7.91 (s, 1H), 7.74-7.61 (m, 2H), 7.15 (dd, *J* = 8.5, 2.3 Hz, 1H), 6.38 (d, *J* = 8.4 Hz, 1H), 4.36 (s, 2H), 4.10 (s, 2H), 3.85 (s, 3H), 3.84 (s, 3H), 2.28 (s, 3H). ¹³C {¹H} NMR (101 MHz, CDCl₃) δ 156.7, 150.4, 147.1, 137.9, 128.6, 128.5, 125.8, 125.5, 122.4, 122.2, 108.8, 62.3, 61.4, 29.3, 12.6.

5-((1,4-dimethoxy-3-methylnaphthalen-2-yl)methyl)pyrimidine (2g). 5 mol% Pd(PPh₃)₄, Eluant (CHX/EtOAc, 5/5, v/v, UV), beige solid, 87% yield. m.p. 104-105 °C. ¹H NMR (500 MHz,

CDCl₃) δ 9.04 (s, 1H), 8.54 (s, 2H), 8.13 – 7.98 (m, 2H), 7.61 – 7.41 (m, 2H), 4.22 (s, 2H), 3.88 (s, 3H), 3.86 (s, 3H), 2.29 (s, 3H). ¹³C {¹H} NMR (126 MHz, CDCl₃) δ 156.9, 156.8, 150.9, 150.8, 133.9, 128.5, 127.3, 126.7, 126.4, 125.9, 122.6, 122.5, 62.5, 61.7, 28.1, 12.9. HRMS (ESI) calcd. for C₁₈H₁₉N₂O₂: 295.1441. Found: 295.1450 (M+H⁺).

2-chloro-5-((1,4-dimethoxy-3-methylnaphthalen-2-yl)methyl)pyrimidine (2h). 2 mol% Pd(PPh₃)₄, Eluant (CHX/EtOAc, 9/1, v/v, UV), white solid, 97% yield. m.p. 88-89 °C. ¹H NMR (400 MHz, CDCl₃) δ 8.43 (s, 2H), 8.13 – 8.00 (m, 2H), 7.61 – 7.43 (m, 2H), 4.18 (s, 2H), 3.88 (s, 3H), 3.85 (s, 3H), 2.29 (s, 3H). ¹³C {¹H} NMR (101 MHz, CDCl₃) δ 159.4, 150.9, 150.7, 132.6, 128.5, 127.2, 126.5, 126.2, 126.0, 125.7, 122.6, 122.5, 62.4, 61.6, 27.3, 12.9. HRMS (ESI) calcd. for C₁₈H₁₈ClN₂O₂: 329.1051. Found: 329.1054 (M+H⁺).

5-((1,4-dimethoxy-3-methylnaphthalen-2-yl)methyl)-2-(trifluoromethyl)pyrimidine (2i). 2 mol% Pd(PPh₃)₄, Eluant (CHX/EtOAc, 8/2, v/v, UV), white solid, 71% yield. ¹H NMR (400 MHz, CDCl₃) δ 8.70 (s, 2H), 8.23 – 7.97 (m, 2H), 7.68 – 7.33 (m, 2H), 4.28 (s, 2H), 3.90 (s, 3H), 3.86 (s, 3H), 2.30 (s, 3H). ¹³C {¹H} NMR (101 MHz, CDCl₃) δ 157.6, 154.9 (q, *J* = 36.8 Hz), 151.0, 150.8, 136.4, 128.6, 127.2, 126.6, 126.1, 125.8, 125.6, 122.6, 122.5, 119.8 (q, *J* = 275.1 Hz), 62.4, 61.6, 28.0, 12.9. ¹⁹F NMR {¹H} (377 MHz, CDCl₃) δ -70.15. HRMS (ESI) calcd. for C₁₉H₁₈F₃N₂O₂: 363.1315. Found: 363.1307 (M+H⁺).

2-((2-methoxypyrimidin-5-yl)methyl)-3-methylnaphthalene-1,4-dione (2j). 2 mol% Pd(PPh₃)₄, Eluant (CHX/EtOAc, 6/4, v/v, UV), translucent oil, 71% yield. **2j** was isolated with an unknown inseparable compound and was used in the next step without any further purification. ¹H NMR (400 MHz, CDCl₃) δ 8.31 (s, 2H), 8.18 – 7.95 (m, 2H), 7.60 – 7.44 (m, 2H), 4.13 (s, 2H), 3.95 (s, 3H), 3.88 (s, 3H), 3.85 (s, 3H), 2.30 (s, 3H). HRMS (ESI) calcd. for C₁₉H₂₀N₂NaO₃: 347.1366. Found: 347.1357 (M+Na⁺).

5-((1,4-dimethoxy-3-methylnaphthalen-2-yl)methyl)pyrimidin-2-amine (2k). 2 mol% Pd(PPh₃)₄, Eluant (CHX/EtOAc, 8/2, v/v, UV), white solid, 80% yield. m. p. 198-200 °C. ¹H NMR (400 MHz, CDCl₃) δ 8.04-8.00 (m, 2H), 7.99 (s, 2H), 7.57-7.51 (m, 2H), 6.45 (s, 2H), 3.97 (s, 2H), 3.83 (s, 3H), 3.78 (s, 3H), 2.26 (s, 3H). ¹³C {¹H} NMR (101 MHz, CDCl₃) δ 162.7, 157.8 (2C), 150.34, 150.30, 129.1, 127.8, 127.1, 126.7, 126.5, 126.3, 122.7, 122.5, 121.5, 62.6, 61.6, 26.8, 12.9. HRMS (ESI) calcd. for C₁₈H₂₀N₃O₂: 310.1550. Found: 310.1539 (M+H⁺).

2-((1,4-dimethoxy-3-methylnaphthalen-2-yl)methyl)furan (2n). 2 mol% Pd(PPh₃)₄, Eluant (CHX/EtOAc, 98/02, v/v, UV), translucent oil, 99% yield. ¹H NMR (400 MHz, CDCl₃) δ 8.19 – 8.03 (m, 2H), 7.62 – 7.46 (m, 2H), 7.34 (dd, *J* = 1.8, 0.9 Hz, 1H), 6.27 (dd, *J* = 3.2, 1.9 Hz, 1H), 5.85 (dq, *J* = 3.2, 1.1 Hz, 1H), 4.27 (s, 2H), 3.92 (s, 3H), 3.90 (s, 3H), 2.41 (s, 3H). ¹³C {¹H} NMR (101 MHz, CDCl₃) δ 154.3, 150.7, 150.4, 141.1, 128.2, 127.3, 127.1, 126.9, 125.9, 125.5, 122.6, 122.3, 110.4, 105.9, 62.6, 61.5, 26.3, 12.4. HRMS (ESI) calcd. for C₁₈H₁₉O₃: 283.1329. Found: 283.1334 (M+H⁺).

5-((1,4-dimethoxy-3-methylnaphthalen-2-yl)methyl)benzo[d]thiazole (2o). 2 mol% Pd(PPh₃)₄, Eluant (CHX/EtOAc, 7/3, v/v, UV), white solid, 81% yield. m.p. = 139-141 °C. ¹H NMR (400 MHz, CDCl₃) δ 8.94 (s, 1H), 8.22-8.04 (m, 2H), 7.89 (s, 1H), 7.82 (d, *J* = 8.3 Hz, 1H), 7.60-7.48 (m, 2H), 7.31 (d, *J* = 8.2 Hz, 1H), 4.46 (s, 2H), 3.88 (s, 3H), 3.87 (s, 3H), 2.31 (s, 3H). ¹³C {¹H} NMR (101 MHz, CDCl₃) δ 154.3, 153.8, 150.7, 150.5, 139.2, 131.3, 128.8, 128.1, 127.3, 126.9, 126.3, 125.9, 125.5, 122.7, 122.5, 122.3, 121.6, 62.4, 61.5, 32.7, 12.8. HRMS (ESI) calcd. for C₂₁H₂₀NO₂S: 350.1209. Found: 350.1202 (M+H⁺).

6-((1,4-dimethoxy-3-methylnaphthalen-2-yl)methyl)benzo[d]thiazole (2p). 2 mol% Pd(PPh₃)₄, Eluant (CHX/EtOAc, 8/2, v/v, UV), colorless oil, 91% yield. ¹H NMR (400 MHz, CDCl₃) δ 8.90 (s, 1H), 8.14-8.10 (m, 2H), 8.03 (d, *J* = 8.4 Hz, 1H), 7.59 (s, 1H), 7.55-7.51 (m, 2H), 7.41-7.37 (m, 1H), 4.43 (s, 2H), 3.87 (s, 3H), 3.86 (s, 3H), 2.28 (s, 3H). ¹³C {¹H} NMR (101

MHz, CDCl₃) δ 153.5, 151.8, 150.8, 150.7, 138.6, 134.3, 128.9, 128.3, 127.4, 127.2, 127.0, 126.1, 125.7, 123.4, 122.7, 122.4, 120.8, 62.5, 61.6, 32.8, 12.9. HRMS (ESI) calcd. for C₂₁H₂₀NO₂S: 350.1209. Found: 350.1210 (M+H⁺).

4-((1,4-dimethoxy-3-methylnaphthalen-2-yl)methyl)pyridine (2q). 5 mol% Pd(PPh₃)₄, Eluant (CHX/EtOAc, 5/5, v/v, UV), yellowish oil, 57% yield. ¹H NMR (400 MHz, CDCl₃) δ 8.52 – 8.40 (m, 2H), 8.23 – 7.97 (m, 2H), 7.68 – 7.40 (m, 2H), 7.14 – 6.99 (m, 2H), 4.26 (s, 2H), 3.86 (s, 3H), 3.83 (s, 3H), 2.23 (s, 3H).

3-((1,4-dimethoxy-3-methylnaphthalen-2-yl)methyl)quinoline (2r). 5 mol% Pd(PPh₃)₄, Eluant (CHX/EtOAc, 7/3, v/v, UV), yellowish solid, 97% yield. m.p. 91-92 °C. ¹H NMR (500 MHz, CDCl₃) δ 8.92 (d, *J* = 2.3 Hz, 1H), 8.17 – 8.10 (m, 2H), 8.07 (dd, *J* = 8.4, 1.0 Hz, 1H), 7.69 – 7.59 (m, 3H), 7.58 – 7.50 (m, 2H), 7.46 (ddd, *J* = 8.1, 6.7, 1.2 Hz, 1H), 4.44 (s, 2H), 3.87 (s, 6H), 2.29 (s, 3H). ¹³C {¹H} NMR (126 MHz, CDCl₃) δ 151.9, 150.9, 150.8, 146.9, 133.9, 133.5, 129.2, 128.8, 128.4, 128.3, 127.9, 127.6, 127.4, 126.7, 126.2, 125.8, 122.7, 122.5, 62.6, 61.6, 30.5, 12.9. HRMS (ESI) calcd. for C₂₃H₂₂NO₂: 344.1645. Found: 344.1659 (M+H⁺).

Post-functionalization of Suzuki coupling adducts.

2-bromo-5-((1,4-dimethoxy-3-methylnaphthalen-2-yl)methyl)pyrimidine (2t). Conditions derived from a previously published procedure (45). To a solution of **2h** (1 equiv., 150 mg, 0.46 mmol) in propionitrile (1.5 mL) was added trimethylbromosilane (2 equiv., 0.12 mL, 0.91 mmol). A white precipitate appeared. The mixture was heated at reflux 5 h and allowed to cool down to room temperature. The mixture was treated with an aqueous saturated sodium bicarbonate solution. The aqueous layer was extracted three times with ethyl acetate, the reunited organic layers were washed with brine, dried over magnesium sulfate, filtered and the solvent was removed under reduced pressure. The product was purified by silica gel chromatography (T/CHX, 95/05, v/v, UV) to afford 2-bromo-5-((1,4-dimethoxy-3-methylnaphthalen-2-yl)methyl)pyrimidine (160 mg, 94%) as a translucent solid. m.p. 99-100 °C. ¹H NMR (500 MHz, CDCl₃) δ 8.37 (s, 2H), 8.11 – 7.98 (m, 2H), 7.65 – 7.47 (m, 2H), 4.16 (s, 2H), 3.88 (s, 3H), 3.85 (s, 3H), 2.29 (s, 3H). ¹³C {¹H} NMR (126 MHz, CDCl₃) δ 159.3, 150.9, 150.8, 150.7, 133.1, 128.5, 127.2, 126.5, 126.17, 126.12, 125.7, 122.6, 122.5, 62.4, 61.7, 27.4, 12.9. HRMS (ESI) calcd. for C₁₈H₁₈BrN₂O₂: 373.0546. Found: 373.0552 (M+H⁺).

5-((1,4-dimethoxy-3-methylnaphthalen-2-yl)methyl)pyrimidine-2-carbonitrile (2u). Conditions derived from a previously published procedure (46). To a solution of sodium cyanide (2 equiv., 44.7 mg, 0.91 mmol) and DABCO (0.2 equiv., 10.8 mg, 0.09 mmol), in a mixture of dimethyl sulfoxide (1.5 mL) and water (0.2 mL), **2h** (1 eq., 150 mg, 0.46 mmol) in dimethyl sulfoxide (1.5 mL) was added dropwise and the reaction mixture was stirred at 50 °C 20 h. After TLC analysis showed complete conversion, the mixture was allowed to cool down to room temperature and was extracted twice with diethyl ether. The reunited organic layers were washed with brine, dried over magnesium sulfate, filtered and the solvent was removed under reduced pressure. The product was purified by silica gel chromatography (CHX/EtOAc, 75/25, v/v, UV) to afford 5-((1,4-dimethoxy-3-methylnaphthalen-2-yl)methyl)pyrimidine-2-carbonitrile (122 mg, 84%) as white solid. m.p. 111-112 °C. ¹H NMR (400 MHz, CDCl₃) δ 8.64 (s, 2H), 8.16 – 7.97 (m, 2H), 7.63 – 7.43 (m, 2H), 4.27 (s, 2H), 3.90 (s, 3H), 3.86 (s, 3H), 2.29 (s, 3H). ¹³C {¹H} NMR (101 MHz, CDCl₃) δ 157.8, 151.1, 150.8, 143.1, 137.2, 128.7, 127.2, 126.7, 126.2, 125.54, 125.52, 122.67, 122.68, 115.9, 62.4, 61.7, 28.3, 12.9. HRMS (ESI) calcd. for C₁₉H₁₈N₃O₂: 320.1394. Found: 320.1403 (M+H⁺).

5-((1,4-dimethoxy-3-methylnaphthalen-2-yl)methyl)-2-((trimethylsilyl)ethynyl)pyrimidine (2v). In a flame dried tube 2-bromo-5-((1,4-dimethoxy-3-

methylnaphthalen-2-yl)methyl)pyrimidine **2t** (1 equiv., 100 mg, 0.27 mmol) was dissolved in triethylamine (8.5 mL) at room temperature under argon. Subsequently, were added in the following order dichlorobis(triphenylphosphine)palladium(II) (0.05 equiv., 11.9 mg, 0.02 mmol), copper iodide (0.1 equiv., 6.4 mg, 0.03 mmol) and ethynyl(trimethyl)silane (3 equiv., 0.14 mL, 1.02 mmol). The mixture was stirred at 70 °C for 24 h. The brown solution turns rapidly into a darker one. The reaction mixture was allowed to return at room temperature then it was quenched with a 1:1 brine:water mixture and the crude of the reaction was extracted three times with ethyl acetate. Reunited organic layers were washed with water, dried over magnesium sulfate, filtered and the solvent was removed under reduced pressure. The crude was purified by silica gel chromatography (CHX/EtOAc, 8/2, v/v, UV) to afford 5-((1,4-dimethoxy-3-methylnaphthalen-2-yl)methyl)-2-((trimethylsilyl)ethynyl)pyrimidine **2e** (104 mg, 99%) as a brown oil. ¹H NMR (400 MHz, CDCl₃) δ 8.49 (s, 2H), 8.13 – 8.03 (m, 2H), 7.58 – 7.47 (m, 2H), 4.21 (s, 2H), 3.85 (s, 3H), 3.85 (s, 3H), 2.26 (s, 3H), 0.27 (s, 9H). ¹³C {¹H} NMR (126 MHz, CDCl₃) δ 156.9, 150.9, 150.8, 150.4, 132.8, 128.4, 127.2, 126.4, 126.3, 125.9, 125.8, 122.6, 122.4, 102.4, 93.8, 62.4, 61.5, 28.0, 12.8, 1.1. HRMS (ESI) calcd. for C₂₃H₂₇N₂O₂Si: 391.1836. Found: 391.1816 (M+H⁺).

5-((1,4-dimethoxy-3-methylnaphthalen-2-yl)methyl)-2-ethynylpyrimidine (2w). 5-((1,4-dimethoxy-3-methylnaphthalen-2-yl)methyl)-2-((trimethylsilyl)ethynyl)pyrimidine **2v** (1 equiv., 323.8 mg, 0.83 mmol) was dissolved in tetrahydrofuran (4.15 mL). Then a solution of tetrabutylammonium fluoride (2.3 equiv., 602 mg, 1.91 mmol) in tetrahydrofuran (4.15 mL) was added dropwise to the original solution and the reaction was stirred during 2 h at room temperature. The reaction was quenched with concentrate solution of ammonium chloride (10 mL) and was extracted three times with ethyl acetate. Reunited organic layers were washed with water, dried over magnesium sulfate, filtered and the solvent was removed under reduced pressure. The crude was purified by silica gel chromatography (CHX/EtOAc, 95/05, v/v, UV) to afford 5-((1,4-dimethoxy-3-methylnaphthalen-2-yl)methyl)-2-ethynylpyrimidine (163.3 mg, 62%) as a brown oil. ¹H NMR (400 MHz, CDCl₃) δ 8.50 (s, 2H), 8.18 – 7.96 (m, 2H), 7.61 – 7.44 (m, 2H), 4.21 (s, 2H), 3.87 (s, 3H), 3.85 (s, 3H), 3.07 (s, 1H), 2.27 (s, 3H). ¹³C {¹H} NMR (126 MHz, CDCl₃) δ 157.1, 150.9, 150.8, 150.0, 133.3, 128.5, 127.2, 126.4, 126.2, 126.0, 125.8, 122.6, 122.5, 81.9, 75.4, 62.4, 61.6, 28.1, 12.9. HRMS (ESI) calcd. for C₂₀H₁₉N₂O₂: 319.1441. Found: 319.1432 (M+H⁺).

Synthesis of the Negishi coupling products **2l** and **2m**

2-((1,4-dimethoxy-3-methylnaphthalen-2-yl)methyl)-5-(trifluoromethyl)pyridine (2l). In a flame dried balloon was charged magnesium (2.3 equiv., 0.22 g, 8.48 mmol) and lithium chloride (1.3 equiv., 0.20 g, 4.79 mmol). Then a 1 M solution of zinc chloride (1.1 equiv., 0.55 g, 4.056 mmol) in dry tetrahydrofuran was added. A solution of 2-(chloromethyl)-1,4-dimethoxy-3-methylnaphthalene (1 equiv., 0.92 g, 3.69 mmol) in dry tetrahydrofuran (9.25 mL) was added and the reaction mixture was stirred at room temperature for 2 h. To a solution of 2-bromo-5-(trifluoromethyl)pyridine (1.2 equiv., 1 g, 4.42 mmol) in dry tetrahydrofuran (9.25 mL) was added successively to the previous mixture and tetrakis(triphenylphosphine)palladium (0.05 equiv., 0.21 g, 0.18 mmol) under argon. The mixture was stirred at 80 °C for 24 h. After cooling down, the reaction mixture was diluted with ethyl acetate and quenched with concentrate solution of ammonium chloride. The phases were separated and the aqueous layer was extracted with ethyl acetate. The crude was extracted three times with ethyl acetate. Reunited organic layers were washed with water, dried over magnesium sulfate, filtered and the solvent was removed under reduced pressure. The crude was purified by silica gel chromatography (CHX/EtOAc, 9/1, v/v, UV) to afford 2-((1,4-dimethoxy-3-methylnaphthalen-2-yl)methyl)-5-(trifluoromethyl)pyridine (702 mg, 52.7%) as a yellow oil. ¹H

NMR (400 MHz, CDCl₃) δ 8.82 (s, 1H), 8.15 – 8.04 (m, 2H), 7.75 – 7.66 (m, 1H), 7.54 – 7.47 (m, 2H), 7.08 (d, *J* = 7.6 Hz, 1H), 4.52 (s, 2H), 3.90 (s, 3H), 3.87 (s, 3H), 2.28 (s, 3H). ¹⁹F NMR {¹H} (377 MHz, CDCl₃) δ -62.22.

2-((1,4-dimethoxy-3-methylnaphthalen-2-yl)methyl)-5-(trifluoromethyl)pyrimidine (2m).

In a flame dried balloon was charged magnesium (2.3 equiv., 24.15 mg, 0.92 mmol) and lithium chloride (1.3 equiv., 21.98 mg, 0.52 mmol). Then a 1 M solution of zinc chloride (1.1 equiv., 59.79 mg, 0.44 mmol) in dry tetrahydrofuran was added. A solution of 2-(chloromethyl)-1,4-dimethoxy-3-methylnaphthalene (1 equiv., 100 mg, 0.4 mmol) in dry tetrahydrofuran (1 mL) was added and the reaction mixture was stirred at room temperature for 2 h. To a solution of 2-chloro-5-(trifluoromethyl)pyrimidine (1.2 equiv., 87.36 mg, 0.48 mmol) in dry tetrahydrofuran (1 mL) was added successively the previous mixture and tetrakis (triphenylphosphine)palladium (0.05 equiv., 23.04 mg, 0.02 mmol) under argon. The mixture was stirred at 80 °C for 24 h. After cooling down, the reaction mixture was diluted with ethyl acetate and quenched with concentrate solution of ammonium chloride. The phases were separated and the aqueous layer was extracted with ethyl acetate. The crude was extracted three times with ethyl acetate. Reunited organic layers were washed with water, dried over magnesium sulfate, filtered and the solvent was removed under reduced pressure. The crude was purified by silica gel chromatography (CHX/EtOAc, 9/1, v/v, UV) to afford 2-((1,4-dimethoxy-3-methylnaphthalen-2-yl)methyl)-5-(trifluoromethyl)pyrimidine (62.4 mg, 43.18%) as a light yellow solid. ¹H NMR (400 MHz, CDCl₃) δ 8.89 (s, 2H), 8.08 (dddd, *J* = 6.7, 4.6, 2.6, 0.7 Hz, 2H), 7.55 – 7.46 (m, 2H), 4.69 (s, 2H), 3.91 (s, 3H), 3.87 (s, 3H), 2.27 (s, 3H). ¹⁹F NMR {¹H} (377 MHz, CDCl₃) δ -62.31.

4,4,5,5-tetramethyl-2-[3-nitro-4-(trifluoromethyl)phenyl]-1,3,2-dioxaborolane (9).

In a sealed tube 4-bromo-2-nitro-1-(trifluoromethyl)benzene (1 equiv., 1 g, 3.7 mmol) and bis(pinacolato)diboron (2.2 equiv., 2 g, 8.15 mmol) were added. Afterwards, dimethylformamide (18.5 mL) was transferred to the flask. To the prepared mixture, potassium acetate (6 equiv., 2.18 g, 22.22 mmol) and (1,1'-Bis(diphenylphosphino)ferrocene) palladium(II) dichloride (0.06 equiv., 0.16 g, 0.22 mmol) were quickly added, the tube was sealed and the mixture was heated to 110 °C for 16 h. After cooling down to room temperature, the black mixture was filtered through a silica and celite pad, washed with ethyl acetate. The crude was extracted three times with ethyl acetate. Reunited organic layers were washed with water, dried over magnesium sulfate, filtered and the solvent was removed under reduced pressure. The crude was purified by silica gel chromatography (CHX/EtOAc, 9/1, v/v, UV) to afford to afford 4,4,5,5-tetramethyl-2-[3-nitro-4-(trifluoromethyl)phenyl]-1,3,2-dioxaborolane (656 mg, 55.8%) as a greenish solid. m.p. 120-122 °C. ¹H NMR (400 MHz, CDCl₃) δ 8.23 (s, 1H), 8.09 (dt, *J* = 7.8, 1.0 Hz, 1H), 7.79 (d, *J* = 7.8 Hz, 1H), 1.35 (s, 12H). ¹³C {¹H} NMR (101 MHz, CDCl₃) δ 147.8, 138.6, 130.6, 127.2 (q, *J* = 5.1 Hz), 125.5 (q, *J* = 34.0 Hz), 122.1 (q, *J* = 273.5 Hz), 85.2, 24.9. ¹⁹F NMR {¹H} (377 MHz, CDCl₃) δ -60.23. HRMS (ESI) not found.

1,4-dimethoxy-2-methyl-3-[[3-nitro-4-(trifluoromethyl)phenyl]methyl]naphthalene (10).

7 mol% Pd(PPh₃)₄, 1.2 equiv. of **9**, Eluant (CHX/EtOAc, 9/1, v/v, UV), yellowish solid, 81% yield. m.p. 114-116 °C. ¹H NMR (400 MHz, CDCl₃) δ 8.16 – 8.04 (m, 2H), 7.70 – 7.63 (m, 2H), 7.60 – 7.48 (m, 2H), 7.46 – 7.37 (m, 1H), 4.36 (s, 2H), 3.87 (d, *J* = 0.8 Hz, 6H), 2.26 (s, 3H). ¹³C {¹H} NMR (101 MHz, CDCl₃) δ 151.0, 150.9, 147.5, 132.0, 128.6, 128.1 (q, *J* = 5.1 Hz), 127.3, 126.6, 126.5, 126.1, 126.0, 124.7, 123.6, 122.7, 122.6, 121.4 (q, *J* = 34.0 Hz), 120.8, 62.5, 61.7, 32.6, 12.9. ¹⁹F NMR {¹H} (377 MHz, CDCl₃) δ -59.77. HRMS (ESI) calcd. for C₂₁H₁₉F₃NO₄:406.1261. Found: 406.1259 (M+H⁺).

2-(3-amino-4-(trifluoromethyl)benzyl)-3-methylnaphthalene-1,4-dione (12).

2-methyl-3-(3-nitro-4-(trifluoromethyl)benzyl)naphthalene-1,4-dione (1 equiv., 297 mg, 0.79 mmol) was dissolved in ethanol (12.3 mL) and ethyl acetate (12.3 mL). Then palladium on carbon (0.1

equiv., 84.22 mg, 0.08 mmol) was added. The mixture was degassed with dihydrogen three times then the reaction was stirred at room temperature overnight under dihydrogen. The solution was filtered through celite, rinsed with ethyl acetate and the filtrate was concentrated under vacuum. The solid was dissolved in acetone (4.4 mL) and stirred at open air during 6 days. The crude was extracted three times with ethyl acetate. Reunited organic layers were washed with water, dried over magnesium sulfate, filtered and the solvent was removed under reduced pressure. The crude oil was purified by silica gel chromatography (CHX/EtOAc, 8/2, v/v, UV) to afford 2-(3-amino-4-(trifluoromethyl)benzyl)-3-methylnaphthalene-1,4-dione (226 mg, 82.7%) as a yellow-orange solid. m.p. 75-78 °C. ¹H NMR (400 MHz, CDCl₃) δ 8.13 – 8.03 (m, 2H), 7.76 – 7.66 (m, 2H), 7.31 (d, *J* = 8.1 Hz, 1H), 6.69 – 6.61 (m, 1H), 6.58 (s, 1H), 4.13 (s, 2H), 3.95 (s, 2H), 2.23 (s, 3H). ¹³C {¹H} NMR (101 MHz, CDCl₃) δ 185.3, 184.7, 144.9, 144.8 (q, *J* = 2.0 Hz), 144.6, 143.4, 133.7 (d, *J* = 1.7 Hz), 132.2, 132.1, 127.1 (q, *J* = 5.1 Hz), 126.6, 126.5, 118.1, 117.0, 112.3 (q, *J* = 30.3 Hz), 32.3, 13.5. ¹⁹F NMR {¹H} (377 MHz, CDCl₃) δ -62.44. HRMS (ESI) calcd. for C₁₉H₁₅F₃NO₂: 346.1049. Found: 346.1043 (M+H⁺).

2-(3-azido-4-(trifluoromethyl)benzyl)-3-methylnaphthalene-1,4-dione (13). 2-(3-amino-4-(trifluoromethyl)benzyl)-3-methylnaphthalene-1,4-dione (1 equiv., 50 mg, 0.14 mmol) was ground in a mortar with 1-methyl-2-oxopyrrolidin-1-ium hydrogen sulfate (4 equiv., 114 mg, 0.58 mmol) and water (0.3 mL) for 1 min. Then sodium nitrite (2.5 equiv., 25 mg, 0.36 mmol) was added and the mixture was ground for 10 min. Finally, sodium azide (2.5 equiv., 23.5 mg, 0.36 mmol) was added to the diazonium salt and grinding continued for 5 min until gas evolution completely stopped. A yellow orange precipitate was formed. The crude was extracted three times with ethyl acetate. Reunited organic layers were washed with water, dried over magnesium sulfate, filtered and the solvent was removed under reduced pressure. The crude was purified by silica gel chromatography (T/CHX with 1% AcOH, 8/2, v/v, UV) to afford 2-(3-azido-4-(trifluoromethyl)benzyl)-3-methylnaphthalene-1,4-dione (20 mg, 37%) as a yellow solid. m.p. 111-113 °C. ¹H NMR (400 MHz, CDCl₃) δ 8.10 (ddd, *J* = 6.1, 5.2, 3.3 Hz, 2H), 7.79 – 7.69 (m, 2H), 7.51 (d, *J* = 8.1 Hz, 1H), 7.19 (s, 1H), 7.04 (d, *J* = 8.0 Hz, 1H), 4.08 (s, 2H), 2.28 (s, 3H). ¹³C {¹H} NMR (101 MHz, CDCl₃) δ 185.2, 184.6, 144.8, 144.72, 144.70, 144.5, 143.3, 133.6, 132.1, 131.9, 126.9 (q, *J* = 5.1 Hz), 126.5, 126.4, 117.9, 116.9, 112.2 (q, *J* = 30.3 Hz), 32.2, 13.3. ¹⁹F NMR {¹H} (377 MHz, CDCl₃) δ -61.64. HRMS (ESI) calcd. for C₁₉H₁₃F₃N₃O₂: 372.0954. Found: 372.0944 (M+H⁺).

Synthesis of the Kochi-Anderson coupling products 3s and 14

2-methyl-3-(thiophen-2-ylmethyl)naphthalene-1,4-dione (3s). Menadione (1 equiv., 100 mg, 0.58 mmol) and 2-thiopheneacetic acid (2 equiv., 165.14 mg, 1.16 mmol) were dissolved in acetonitrile (9 mL) and water (3 mL). The mixture was heated to 85 °C and silver nitrate (0.35 equiv., 34.53 mg, 0.20 mmol) with ammonium persulfate (0.35 equiv., 172.29 mg, 0.76 mmol) were added. The reaction was stirred for 4 h at 85 °C in the dark. The solvent was removed in vacuum and then extracted three times with ethyl acetate. Reunited organic layers were washed with water, dried over magnesium sulfate, filtered and the solvent was removed under reduced pressure. The crude oil was purified by silica gel chromatography (T/CHX, 7/3, v/v, UV) to afford 2-methyl-3-(4-nitrobenzyl)naphthalene-1,4-dione (115 mg, 75%) as yellow solid). m.p. = 96-97 °C. ¹H NMR (CDCl₃, 400 MHz) δ 8.11-8.03 (m, 2H), 7.71-7.65 (m, 2H), 7.11 (dd, *J* = 4.5, 1.8 Hz, 1H), 6.89 (d, *J* = 4.5 Hz, 2H), 4.18 (s, 2H), 2.29 (s, 3H). ¹³C {¹H} NMR (CDCl₃, 101 MHz) δ 185.3, 184.2, 144.4, 144.1, 139.9, 133.61, 133.59, 132.1, 132.0, 126.9, 126.5, 126.4, 125.8, 124.2, 27.0, 13.1. HRMS (ESI) calcd. for C₁₆H₁₂NaO₂S: 291.0450. Found: 291.0455 (M+Na⁺).

2-methyl-3-(4-nitrobenzyl)naphthalene-1,4-dione (14). Menadione (1 equiv., 500 mg, 2.9 mmol) and 4-nitrophenylacetic acid (2 equiv., 1.05 g, 5.81 mmol) were dissolved in acetonitrile (44.9 mL) and water (14.9 mL). The mixture was heated to 85 °C and silver nitrate (0.35 equiv., 172.6 mg, 1.0 mmol) with ammonium persulfate (0.35 equiv., 861.4 mg, 3.8 mmol) were added. The reaction was stirred for 4 h at 85 °C in the dark. The solvent was removed in vacuum and then extracted three times with ethyl acetate. Reunited organic layers were washed with water, dried over magnesium sulfate, filtered and the solvent was removed under reduced pressure. The crude oil was purified by silica gel chromatography (T/CHX, 7/3, v/v, UV) to afford 2-methyl-3-(4-nitrobenzyl)naphthalene-1,4-dione (839.2 mg, 94%) as a yellow solid. m.p. 153-154 °C. ¹H NMR (400 MHz, CDCl₃) δ 8.22 – 8.03 (m, 4H), 7.79 – 7.61 (m, 2H), 7.44 – 7.31 (m, 2H), 4.13 (s, 2H), 2.26 (s, 3H). ¹³C {¹H} NMR (101 MHz, CDCl₃) δ 185.1, 184.5, 146.8, 145.9, 145.3, 143.9, 133.9, 133.8, 132.2, 131.9, 129.5, 126.7, 126.6, 124.1, 32.6, 13.6. HRMS (ESI) calcd. for C₁₈H₁₄NO₄: 308.0917. Found: 308.0923 (M+H⁺).

2-(4-aminobenzyl)-3-methylnaphthalene-1,4-dione (15). 2-methyl-3-(4-nitrobenzyl)naphthalene-1,4-dione (1 equiv., 276 mg, 0.9 mmol) was dissolved in ethanol (14 mL) and ethyl acetate (14 mL). Then palladium on carbon (0.1 equiv., 95.6 mg, 0.09 mmol) was added. The mixture was degassed with dihydrogen three times then the reaction was stirred at room temperature overnight under dihydrogen. The solution was filtered through celite, rinsed with ethyl acetate and the filtrate was concentrated under vacuum. The solid was dissolved in acetone (10 mL) and stirred at open air during 6 days. The crude was extracted three times with ethyl acetate. Reunited organic layers were washed with water, dried over magnesium sulfate, filtered and the solvent was removed under reduced pressure. The crude oil was purified by silica gel chromatography (CHX/EtOAc, 8/2, v/v, UV) to afford 2-(4-aminobenzyl)-3-methylnaphthalene-1,4-dione (187.8 mg, 75%) as an orange solid. m.p. 55-57 °C. ¹H NMR (400 MHz, CDCl₃) δ 8.08 (ddt, *J* = 6.0, 3.2 Hz, 2H), 7.68 (dd, *J* = 5.7, 3.3 Hz, 2H), 7.06 – 6.96 (m, 2H), 6.65 – 6.55 (m, 2H), 3.91 (s, 2H), 3.58 (s, 2H), 2.25 (s, 3H). ¹³C {¹H} NMR (101 MHz, CDCl₃) δ 185.7, 184.9, 146.0, 144.9, 144.0, 133.54, 133.50, 132.3, 132.2, 129.7, 128.0, 126.6, 126.3, 115.5, 31.7, 13.3. HRMS (ESI) calcd. for C₁₈H₁₆NO₂: 278.1175. Found: 278.1179 (M+H⁺).

2-(4-azidobenzyl)-3-methylnaphthalene-1,4-dione (16). 2-(4-aminobenzyl)-3-methylnaphthalene-1,4-dione (1 equiv., 100 mg, 0.36 mmol) was ground in a mortar using a pestle with 1-methyl-2-oxopyrrolidin-1-ium hydrogen sulfate (4 equiv., 284.4 mg, 1.44 mmol) and water (0.7 mL) for 1 min. Then sodium nitrite (2.5 equiv., 62.2 mg, 0.9 mmol) was added and the mixture was ground for 10 min. Finally, sodium azide (2.5 equiv., 58.6 mg, 0.9 mmol) was added to the diazonium salt and grinding continued for 5 min until gas evolution completely stopped. An orange precipitate was formed. The crude was extracted three times with ethyl acetate. Reunited organic layers were washed with water, dried over magnesium sulfate, filtered and the solvent was removed under reduced pressure. The crude was purified by silica gel chromatography (CHX/EtOAc, 8/2, v/v, UV) to afford 2-(4-azidobenzyl)-3-methylnaphthalene-1,4-dione (90.3 mg, 83%) as an orange solid. m.p. 60-62 °C. ¹H NMR (400 MHz, CDCl₃) δ 8.09 (dt, *J* = 6.0, 3.2 Hz, 2H), 7.70 (dd, *J* = 5.8, 3.3 Hz, 2H), 7.26 – 7.18 (d, 2H), 6.98 – 6.89 (d, 2H), 4.00 (s, 2H), 2.25 (s, 3H). ¹³C {¹H} NMR (101 MHz, CDCl₃) δ 185.4, 184.8, 145.1, 144.5, 138.4, 134.9, 133.7, 132.2, 132.1, 130.1, 126.6, 126.5, 119.4, 32.0, 13.4. HRMS (ESI) calcd. for C₁₈H₁₄N₃O₂: 304.1080. Found: 304.1071 (M+H⁺).

General procedure for the oxidative deprotection.

1,4-dimethoxy-3-benzylmenadion derivatives (1 equiv.) was dissolved in stirring acetonitrile (0.08 M). Then, at room temperature, CAN (2.1 equiv.) dissolved in water (0.25 M) was added drop by drop. The mixture was stirred at room temperature during 1 h. Then after TLC analysis

showed complete conversion, the aqueous layer was extracted three times with dichloromethane. Combined organic layers were dried over magnesium sulfate, filtered and the solvent was removed under reduced pressure. Purification by silica gel chromatography was performed using the adequate eluent.

2-methyl-3-(pyridin-3-ylmethyl)naphthalene-1,4-dione (3a). Eluant (CHX/EtOAc, 5/5, v/v, UV), yellow solid, 74% yield. m.p. 100-101 °C. ¹H NMR (400 MHz, CDCl₃) δ 8.54 – 8.51 (m, 1H), 8.43 (dd, *J* = 4.8, 1.6 Hz, 1H), 8.16 – 7.97 (m, 2H), 7.70 (dd, *J* = 5.8, 3.3 Hz, 2H), 7.54 (ddd, *J* = 7.9, 2.4, 1.6 Hz, 1H), 7.18 (ddd, *J* = 7.8, 4.8, 0.9 Hz, 1H), 4.01 (s, 2H), 2.25 (s, 3H). ¹³C {¹H} NMR (101 MHz, CDCl₃) δ 185.2, 184.6, 150.0, 148.0, 144.8, 144.4, 136.2, 133.9, 133.85, 133.83, 132.2, 131.9, 126.6, 126.5, 123.7, 30.0, 13.4. HRMS (ESI) calcd. for C₁₇H₁₄NO₂: 264.1019. Found: 264.1018 (M+H⁺).

2-methyl-3-((6-(trifluoromethyl)pyridin-3-yl)methyl)naphthalene-1,4-dione (3b). Eluant (CHX/EtOAc, 8/2, v/v, UV), yellow solid, 87% yield. m.p. 108-109 °C. ¹H NMR (500 MHz, CDCl₃) δ 8.66 (d, *J* = 2.2 Hz, 1H), 8.20 – 7.97 (m, 2H), 7.89 – 7.68 (m, 3H), 7.58 (dd, *J* = 8.1, 0.8 Hz, 1H), 4.09 (s, 2H), 2.28 (s, 3H). ¹³C {¹H} NMR (126 MHz, CDCl₃) δ 184.9, 184.4, 150.3, 146.6 (q, *J* = 34.8 Hz), 145.2, 143.5, 137.5, 137.4, 133.94, 133.92, 132.1, 131.9, 126.7, 126.6, 121.6 (q, *J* = 279.6 Hz), 120.5 (q, *J* = 2.7 Hz), 30.0, 13.6. ¹⁹F NMR {¹H} (471 MHz, CDCl₃) δ -67.81. HRMS (ESI) calcd. for C₁₈H₁₃F₃NO₂: 332.0893. Found: 332.0915 (M+H⁺).

2-((6-fluoropyridin-3-yl)methyl)-3-methylnaphthalene-1,4-dione (3c). Eluant (CHX/EtOAc, 8/2, v/v, UV), yellow solid, 97% yield. m.p. 103-104 °C. ¹H NMR (500 MHz, CDCl₃) δ 8.13 (d, *J* = 2.6 Hz, 1H), 8.08 (ddd, *J* = 7.4, 5.8, 3.3 Hz, 2H), 7.72 (dd, *J* = 5.8, 3.3 Hz, 2H), 7.67 (td, *J* = 8.1, 2.6 Hz, 1H), 6.84 (dd, *J* = 8.4, 3.0 Hz, 1H), 4.00 (s, 2H), 2.27 (s, 3H). ¹³C {¹H} NMR (126 MHz, CDCl₃) δ 185.1, 184.6, 162.6 (d, *J* = 238.4 Hz), 147.5 (d, *J* = 14.7 Hz), 144.8, 144.2, 141.5 (d, *J* = 7.8 Hz), 133.97, 133.92, 132.1, 131.9, 131.5 (d, *J* = 4.7 Hz), 126.65, 126.61, 109.6 (d, *J* = 37.5 Hz), 29.1, 13.4. ¹⁹F NMR {¹H} (377 MHz, CDCl₃) δ -70.88 (d, *J* = 7.7 Hz). HRMS (ESI) calcd. for C₁₇H₁₃FNO₂: 282.0925. Found: 282.0920 (M+H⁺).

2-((6-chloropyridin-3-yl)methyl)-3-methylnaphthalene-1,4-dione (3d). Eluant (CHX/EtOAc, 8/2, v/v, UV), yellow solid, 99% yield. m.p. 120-121 °C. ¹H NMR (500 MHz, CDCl₃) δ 8.30 (d, *J* = 2.5 Hz, 1H), 8.11 – 7.96 (m, 2H), 7.75 – 7.63 (m, 2H), 7.51 (dd, *J* = 8.2, 2.6 Hz, 1H), 7.20 (d, *J* = 8.2 Hz, 1H), 3.97 (s, 2H), 2.25 (s, 3H). ¹³C {¹H} NMR (126 MHz, CDCl₃) δ 184.9, 184.4, 149.8, 149.7, 144.9, 143.9, 139.1, 133.9, 133.8, 132.9, 132.1, 131.9, 126.6, 126.5, 124.3, 29.3, 13.4. HRMS (ESI) calcd. for C₁₇H₁₃ClNO₂: 298.0629. Found: 298.0648 (M+H⁺).

2-((6-methoxypyridin-3-yl)methyl)-3-methylnaphthalene-1,4-dione (3e). Eluant (CHX/EtOAc, 9/1, v/v, UV), yellow solid, 87% yield. m.p. 120-121 °C. ¹H NMR (400 MHz, CDCl₃) δ 8.11 – 7.95 (m, 3H), 7.67 (dd, *J* = 5.8, 3.3 Hz, 2H), 7.50 (dd, *J* = 8.6, 2.5 Hz, 2H), 6.67 (d, *J* = 8.6 Hz, 1H), 3.91 (s, 2H), 3.88 (s, 3H), 2.24 (s, 3H). ¹³C {¹H} NMR (101 MHz, CDCl₃) δ 185.2, 184.6, 162.8, 145.9, 144.7, 144.4, 139.9, 133.77, 133.74, 132.1, 131.9, 126.7, 126.5, 126.4, 111.0, 53.8, 29.0, 13.3. HRMS (ESI) calcd. for C₁₈H₁₅NO₃: 294.1125. Found: 294.1125 (M+H⁺).

2-((6-aminopyridin-3-yl)methyl)-3-methylnaphthalene-1,4-dione (3f). Eluant (EtOAc, 10, v/v, UV), orange solid, 68% yield. m.p. 122-124 °C. ¹H NMR (400 MHz, CDCl₃) δ 8.08 (dt, *J* = 5.9, 3.0 Hz, 2H), 7.95 (s, 1H), 7.76-7.60 (m, 2H), 7.35 (dd, *J* = 8.5, 2.3 Hz, 1H), 6.44 (d, *J* = 8.5 Hz, 1H), 4.59 (s, 2H), 3.86 (s, 2H), 2.26 (s, 3H). ¹³C {¹H} NMR (101 MHz, CDCl₃) δ 185.4, 184.8, 156.9, 146.8, 145.0, 144.3, 139.0, 133.7, 132.2, 132.1, 126.6, 126.5, 109.3, 29.1, 13.3.

2-methyl-3-(pyrimidin-5-ylmethyl)naphthalene-1,4-dione (3g). Eluant (CHX/EtOAc, 5/5, v/v, UV), yellow solid, 88% yield. m.p. 110-111 °C. ¹H NMR (500 MHz, CDCl₃) δ 9.04 (s, 1H),

8.64 (s, 2H), 8.10 – 7.98 (m, 2H), 7.76 – 7.61 (m, 2H), 3.98 (s, 2H), 2.27 (s, 3H). ¹³C {¹H} NMR (126 MHz, CDCl₃) δ 184.8, 184.3, 157.2, 157.0, 145.1, 143.2, 133.96, 133.92, 132.07, 132.04, 131.8, 126.6, 27.8, 13.5. HRMS (ESI) calcd. for C₁₆H₁₃N₂O₂: 265.0972. Found: 265.0982 (M+H⁺).

2-((2-chloropyrimidin-5-yl)methyl)-3-methylnaphthalene-1,4-dione (3h). Eluant (CHX/EtOAc, 7/3, v/v, UV), yellow solid, 93% yield. m.p. 163-164 °C. ¹H NMR (400 MHz, CDCl₃) δ 8.54 (s, 2H), 8.20 – 7.92 (m, 2H), 7.85 – 7.57 (m, 2H), 3.96 (s, 2H), 2.29 (s, 3H). ¹³C {¹H} NMR (101 MHz, CDCl₃) δ 184.6, 184.1, 159.7, 159.6, 145.1, 142.6, 133.96, 133.97, 131.9, 131.6, 130.6, 126.6, 126.5, 27.1, 13.5. HRMS (ESI) calcd. for C₁₆H₁₂ClN₂O₂: 299.0582. Found: 299.0596 (M+H⁺).

2-methyl-3-((2-(trifluoromethyl)pyrimidin-5-yl)methyl)naphthalene-1,4-dione (3i). Eluant (CHX/EtOAc, 8/2, v/v, UV), yellow solid, 95% yield. m.p. 195-196 °C. ¹H NMR (400 MHz, CDCl₃) δ 8.82 (s, 2H), 8.25 – 8.01 (m, 2H), 7.84 – 7.65 (m, 2H), 4.08 (s, 2H), 2.32 (s, 3H). ¹³C {¹H} NMR (101 MHz, CDCl₃) δ 184.6, 184.2, 158.0, 155.3 (q, *J* = 37.1 Hz), 145.5, 142.4, 134.4, 134.2, 134.1, 132.1, 131.7, 126.8, 126.7, 119.7 (q, *J* = 275.1 Hz), 27.9, 13.7. ¹⁹F NMR {¹H} (377 MHz, CDCl₃) δ -70.23. HRMS (ESI) calcd. for C₁₇H₁₂F₃N₂O₂: 333.0845. Found: 333.0868 (M+H⁺).

2-((2-methoxypyrimidin-5-yl)methyl)-3-methylnaphthalene-1,4-dione (3j). Eluant (CHX/EtOAc, 7/3, v/v, UV), yellow solid, 74% yield. m.p. 161-162 °C. ¹H NMR (400 MHz, CDCl₃) δ 8.40 (s, 2H), 8.10 – 7.96 (m, 2H), 7.67 (dd, *J* = 5.8, 3.3 Hz, 2H), 3.92 (s, 3H), 3.87 (s, 2H), 2.25 (s, 3H). ¹³C {¹H} NMR (101 MHz, CDCl₃) δ 184.9, 184.3, 164.6, 159.2, 144.5, 143.8, 133.86, 133.82, 132.0, 131.8, 126.57, 126.54, 124.9, 54.9, 26.7, 13.4. HRMS (ESI) calcd. for C₁₇H₁₅N₂O₃: 295.1077. Found: 295.1087 (M+H⁺).

2-((2-aminopyrimidin-5-yl)methyl)-3-methylnaphthalene-1,4-dione (3k). (DCM/MeOH, 9/1, v/v, UV), orange solid, 60% yield. m.p. = degradation after 200 °C. ¹H NMR (500 MHz, DMSO) δ 8.12 (s, 2H), 8.01 – 7.96 (m, 2H), 7.84 – 7.80 (m, 2H), 6.46 (s, 2H), 3.73 (s, 2H), 2.18 (s, 3H). ¹³C {¹H} (126 MHz, DMSO) δ 184.6, 184.2, 162.4, 144.1, 143.8, 133.9, 133.8, 131.7, 131.5, 125.9, 125.8, 119.5, 13.0. HRMS (ESI) calcd. for C₁₆H₁₄N₃O₂: 290.1081. Found: 280.1081 (M+H⁺).

2-methyl-3-((5-(trifluoromethyl)pyridin-2-yl)methyl)naphthalene-1,4-dione (3l). Eluant (CHX/EtOAc, 9/1, v/v, UV), yellow solid, 14% yield. ¹H NMR (400 MHz, CDCl₃) δ 8.72 (s, 1H), 8.14 – 8.02 (m, 2H), 7.86 – 7.78 (m, 1H), 7.74 – 7.62 (m, 2H), 7.46 – 7.38 (m, 1H), 4.27 (s, 2H), 2.30 (s, 3H). ¹⁹F NMR {¹H} (377 MHz, CDCl₃) δ -62.36.

2-methyl-3-((5-(trifluoromethyl)pyrimidin-2-yl)methyl)naphthalene-1,4-dione (3m). Eluant (CHX/EtOAc, 8/2, v/v, UV) yellow solid, 47% yield. ¹H NMR (400 MHz, CDCl₃) δ 8.86 (s, 2H), 8.16 – 8.02 (m, 2H), 7.75 – 7.65 (m, 2H), 4.46 (s, 2H), 2.21 (s, 3H). ¹⁹F NMR {¹H} (377 MHz, CDCl₃) δ -62.38.

2-(furan-2-ylmethyl)-3-methylnaphthalene-1,4-dione (3n). Eluant (CHX/EtOAc, 98/02, v/v, UV), orange solid, 74% yield. m.p. 83-84 °C. ¹H NMR (400 MHz, CDCl₃) δ 8.21 – 7.95 (m, 2H), 7.86 – 7.58 (m, 2H), 7.27 (dd, *J* = 1.9, 0.9 Hz, 1H), 6.26 (dd, *J* = 3.2, 1.9 Hz, 1H), 6.07 (dd, *J* = 3.2, 0.9 Hz, 1H), 4.03 (s, 2H), 2.28 (s, 3H). ¹³C {¹H} NMR (101 MHz, CDCl₃) δ 185.3, 184.1, 151.3, 145.0, 142.4, 141.6, 133.6, 133.6, 132.2, 132.0, 126.6, 126.4, 110.5, 106.8, 25.6, 13.1.

2-(benzo[d]thiazol-5-ylmethyl)-3-methylnaphthalene-1,4-dione (3o). Eluant (CHX/EtOAc, 8/2, v/v, UV), yellow solid, 78% yield. m.p. = 148-149 °C. ¹H NMR (CDCl₃, 400 MHz) δ 8.97 (s, 1H), 8.06 (dt, *J* = 5.7, 3.1 Hz, 2H), 7.95 (s, 1H), 7.85 (d, *J* = 8.2 Hz, 1H), 7.83-7.57 (m, 1H), 7.36 (d, *J* = 8.1 Hz, 2H), 4.18 (s, 2H), 2.27 (s, 3H). ¹³C {¹H} NMR (CDCl₃, 101 MHz) δ 185.3,

184.6, 154.8, 153.9, 145.0, 144.8, 136.6, 133.6 (2C), 132.1 (2C), 132.0, 126.7, 126.5, 126.4, 123.1, 122.0, 32.3, 13.4. HRMS (ESI) calcd. for C₁₉H₁₃NNaO₂S: 342.0559. Found: 342.0555 (M+Na⁺).

2-(benzo[d]thiazol-6-ylmethyl)-3-methylnaphthalene-1,4-dione (3p). Eluant (CHX/EtOAc, 8/2, v/v, UV), yellow solid, 78% yield. m.p. = 146-147 °C. ¹H NMR (CDCl₃, 400 MHz) δ 8.95 (s, 1H), 8.15-8.06 (m, 2H), 8.04 (d, *J* = 8.3 Hz, 1H), 7.81 (s, 1H), 7.71 (dd, *J* = 5.7, 3.3 Hz, 2H), 7.42 (d, *J* = 7.8 Hz, 1H), 4.19 (s, 2H), 2.29 (s, 3H). ¹³C {¹H} NMR (CDCl₃, 101 MHz) δ 185.3, 184.7, 154.3, 152.4, 144.9, 144.7, 135.9, 134.8, 133.65, 133.64, 132.1, 132.0, 127.3, 126.6, 126.4, 123.6, 121.5, 32.4, 13.5. HRMS (ESI) calcd. for C₁₉H₁₄NO₂S: 320.0740 Found: 320.0740 (M+H⁺).

2-methyl-3-(pyridin-4-ylmethyl)naphthalene-1,4-dione (3q). Compound **3q** was not purified, yellow solid, 96% yield. ¹H NMR (400 MHz, CDCl₃) δ 8.64 (s, 2H), 8.27 – 7.96 (m, 2H), 7.87 – 7.71 (m, 2H), 7.64 (s, 2H), 4.21 (s, 2H), 2.29 (s, 3H). ¹³C {¹H} NMR (101 MHz, CDCl₃) δ 184.5, 184.2, 156.2, 146.4, 143.4, 141.8, 134.3, 134.2, 132.1, 131.6, 126.86, 126.83, 126.3, 33.2, 13.9.(17)

2-methyl-3-(quinolin-3-ylmethyl)naphthalene-1,4-dione (3r). Eluant (CHX/EtOAc, 5/5, v/v, UV), yellow solid, 86% yield. m.p. 190-191 °C. ¹H NMR (400 MHz, CDCl₃) δ 8.87 (d, *J* = 2.2 Hz, 1H), 8.14 – 8.06 (m, 2H), 8.05 (dd, *J* = 8.5, 1.0 Hz, 1H), 7.92 (dd, *J* = 2.3, 1.0 Hz, 1H), 7.75 – 7.68 (m, 3H), 7.64 (ddd, *J* = 8.4, 6.9, 1.5 Hz, 1H), 7.49 (ddd, *J* = 8.1, 6.8, 1.2 Hz, 1H), 4.20 (s, 2H), 2.31 (s, 3H). ¹³C {¹H} NMR (101 MHz, CDCl₃) δ 185.2, 184.6, 151.7, 147.1, 144.9, 144.4, 134.8, 133.8, 133.8, 132.2, 132.0, 131.1, 129.3, 129.2, 128.1, 127.6, 126.9, 126.6, 126.5, 30.2, 13.6. HRMS (ESI) calcd. for C₂₁H₁₆NO₂: 314.1176. Found: 314.1177 (M+H⁺).

2-((2-bromopyrimidin-5-yl)methyl)-3-methylnaphthalene-1,4-dione (3t). Eluant (CHX/EtOAc, 75/25, v/v, UV), yellow solid, 96% yield. m.p. 165-166 °C. ¹H NMR (400 MHz, CDCl₃) δ 8.48 (s, 2H), 8.11 – 8.00 (m, 2H), 7.80 – 7.60 (m, 2H), 3.94 (s, 2H), 2.28 (s, 3H). ¹³C {¹H} NMR (101 MHz, CDCl₃) δ 184.7, 184.2, 159.6, 151.3, 145.2, 142.7, 134.1, 134.0, 132.0, 131.7, 131.1, 126.78, 126.74, 27.2, 13.6. HRMS (ESI) calcd. for C₁₆H₁₂BrN₂O₂: 343.0077. Found: 343.0099 (M+H⁺).

5-((3-methyl-1,4-dioxo-1,4-dihydronaphthalen-2-yl)methyl)pyrimidine-2-carbonitrile (3u). Eluant (CHX/EtOAc, 7/3, v/v, UV), yellow solid, 87% yield. m.p. 179-180 °C. ¹H NMR (400 MHz, CDCl₃) δ 8.76 (s, 2H), 8.10 – 7.99 (m, 2H), 7.81 – 7.61 (m, 2H), 4.06 (s, 2H), 2.31 (s, 3H). ¹³C {¹H} NMR (101 MHz, CDCl₃) δ 184.5, 184.2, 158.1, 145.7, 143.4, 142.0, 135.2, 134.2, 134.1, 132.0, 131.6, 126.8, 126.7, 115.7, 28.2, 13.7. HRMS (ESI) calcd. for C₁₇H₁₂N₃O₂: 290.0924. Found: 290.0918 (M+H⁺).

2-((2-ethynylpyrimidin-5-yl)methyl)-3-methylnaphthalene-1,4-dione (3v). Eluant (CHX/EtOAc, 8/2, v/v, UV), yellow solid, 72% yield. m.p. 160-162 °C. ¹H NMR (500 MHz, CDCl₃) δ 8.63 (s, 2H), 8.13 – 7.99 (m, 2H), 7.81 – 7.61 (m, 2H), 3.99 (s, 2H), 3.09 (s, 1H), 2.28 (s, 3H). ¹³C {¹H} NMR (126 MHz, CDCl₃) δ 184.8, 184.3, 157.4, 150.4, 145.2, 142.8, 134.1, 133.9, 132.1, 131.8, 131.4, 126.7, 81.7, 75.9, 27.9, 13.6. HRMS (ESI) calcd. for C₁₈H₁₃N₂O₂: 289.0971. Found: 289.0967 (M+H⁺).

2-(4-ethynylbenzyl)-3-methylnaphthalene-1,4-dione (8). Eluant (CHX/EtOAc, 8/2, v/v, UV), yellow solid, 46% overall yield (over 5 steps). ¹H NMR (400 MHz, CDCl₃) δ 8.18 – 8.03 (m, 2H), 7.71 (dd, *J* = 5.8, 3.3 Hz, 2H), 7.44 – 7.30 (m, 2H), 7.22 – 7.14 (m, 2H), 4.03 (s, 2H), 3.03 (s, 1H), 2.23 (s, 3H). Conform to the previous publication (14).

2-methyl-3-(3-nitro-4-(trifluoromethyl)benzyl)naphthalene-1,4-dione (11). Eluant (CHX/EtOAc, 8/2, v/v, UV), yellow solid, 82% yield. m.p. 155-158 °C. ¹H NMR (400 MHz,

CDCl₃) δ 8.21 – 8.04 (m, 2H), 7.79 – 7.69 (m, 4H), 7.59 (ddt, *J* = 7.2, 1.7, 0.9 Hz, 1H), 4.14 (s, 2H), 2.28 (s, 3H). ¹³C {¹H} NMR (101 MHz, CDCl₃) δ 184.8, 184.4, 145.6, 144.8, 143.0, 134.1, 134.0, 132.7, 132.1, 131.8, 128.4 (q, *J* = 5.2 Hz), 126.8, 126.7, 125.1, 123.4, 122.1 (q, *J* = 34.0 Hz), 120.7, 32.4, 13.7. ¹⁹F NMR {¹H} (377 MHz, CDCl₃) δ -59.88. HRMS (ESI) calcd. for C₁₉H₁₃F₃NO₄: 376.0791. Found: 376.0791 (M+H⁺).

***Plasmodium falciparum* assays and bioimaging**

Parasite culture and antiplasmodial assays. The *P. falciparum* growth inhibition assay was used to determine the 50% inhibitory concentration (IC₅₀) of a given compound. Compounds were dissolved in DMSO at 10 mM. The stocks were kept at 4 °C for usually ≥2 weeks. For the assay, 4-fold concentrated solutions of all compounds were prepared freshly in screening medium. The *P. falciparum* growth inhibition assay method described here was based on the published protocol (24). The readout method is based on incorporation of radiolabelled hypoxanthine into the parasites DNA, which serves as indicator of parasite growth (24,47). In brief, naïve parasites of strain NF54 were exposed to a serial dilution of compounds for 72 hours. After 48 h, a [³H]-hypoxanthine (0.25 μCi) solution is added to each well, and the plates are incubated for another 24 h. Plates are harvested with a Betaplate cell harvester (Perkin, Elmer, Waltham, US), which transfers the lysed red blood cells onto a glass fiber filter (Microbeta FilterMate). The dried filters are inserted into plastic foil with 10 mL of scintillation fluid and counted in a Betaplate liquid scintillation counter (Perkin Elmer, Waltham, US). The results are recorded as counts *per minute per well* at each compound concentration. Data are transferred into a graphics program (e.g., Excel) and expressed as percentage of the values for untreated controls (24,47). Chloroquine Diphosphate (Sigma C6628) and Artesunate (Mepha) were included as reference compound(s) in every experiment.

Parasite culture for bioimaging. Parasites were maintained in fresh A+ human red blood cells at a 3% hematocrit in complete medium: RPMI 1640 (Gibco, ref 72400-021) supplemented with 25 mM HEPES, 0.25 % Albumax II (Thermo Fisher, ref 11021029), 5 % inactivated human serum, 2X hypoxanthine (C.C.pro, ref z-41-M), and 10 μg/mL gentamicin (Gibco, ref 15710-064). Cultures were incubated at 37 °C in a humidified atmosphere with 5% O₂, 5% CO₂, and 90% N₂.

3-Benzylmenadione probe localisation. *P. falciparum* NF54 trophozoites (5% parasitemia, 1.5% hematocrit) were subjected to incubation with probes **3v** and **8** at a concentration of 10 μM for 2 h. Subsequently, dual Click chemistry and immuno-staining procedures were conducted on fixed blood smears following the described protocol (48), albeit with some modifications. In brief, thin blood smears were fixed using 4% (w/v) paraformaldehyde in PBS for 10 min at RT, and then permeabilized for 10 min using 0.1% Triton X-100 in PBS. The Click reaction was carried out for 30 minutes at room temperature using 5 μM of Alexa Fluor 488 Azide (Thermo Fisher Scientific, ref A10266) in the presence of CuSO₄ and the "Click-it" Cell Reaction Buffer Kit (Thermo Fisher Scientific, ref C10269) following the manufacturer's instructions. The samples then underwent co-staining with antibodies specific to mitochondria and apicoplast. The smears were first blocked with 3% (w/v) BSA in PBS for 15 minutes and then incubated with either (i) mouse polyclonal antibodies against the mitochondrial protein PfHSP60 (1:500 in 3% BSA) (kindly provided by Philippe Grellier, Muséum National d'Histoire Naturelle, Paris) followed by goat anti-mouse IgG conjugated with Alexa Fluor 647 (Thermo Fisher Scientific, ref A21235, 1:1000 in 3% BSA), or (ii) rabbit polyclonal antibodies against *Toxoplasma gondii* CPN60 (1:500 in 3% BSA, cross-reacting with PfCPN60) (49) followed by goat anti-rabbit IgG conjugated with Alexa Fluor 647 (Thermo Fisher Scientific, ref A21244, 1:1000 in 3% BSA). Parasite nuclei were stained with DAPI (Thermo Scientific, ref 62248, 1:1000 in PBS) for 5 min at RT. Finally, the slides were mounted in Immu-Mount (Eprelia, ref 9990402).

Morphological modifications after treatment with 3-benzylmenadiones. *P. falciparum* NF54 trophozoites (1.5% parasitemia, 1.5% hematocrit) were subjected to incubation with **PD** and probe **8** at their IC_{50} concentration (50 nM) for 14 and 48 h. Thin blood smears were fixed using 4% (w/v) paraformaldehyde in PBS for 10 min at RT, permeabilized for 10 min using 0.1% Triton X-100 in PBS, and blocked with 3% (w/v) BSA in PBS for 15 min. The samples were then co-stained with a mix of antibodies specific to mitochondria and apicoplast (same as above) followed by incubation with cocktail of goat anti-mouse IgG conjugated with Alexa Fluor 647 (Thermo Fisher Scientific, ref A21235, 1:1000 in 3% BSA), and goat anti-rabbit IgG conjugated with Alexa Fluor 488 (Thermo Fisher Scientific, ref A11008 1:1000 in 3% BSA). Parasite nuclei were stained with DAPI (Thermo Scientific, ref 62248, 1:1000 in PBS) for 5 min at RT, and the slides were mounted in Immu-Mount (Epredia, ref 9990402).

Image acquisition and analysis. Imaging was performed using a Zeiss LSM 980 Airyscan 2 laser-scanning microscope built around an Axio Observer 7 body and equipped with an Airyscan 2 super-resolution detector, and controlled by Zen Blue 3.8 software. Image processing was conducted using Fiji software (ImageJ2, version 2.14.0/1.54f), and the final figures were compiled using the Quickfigures plugin. Probe association with a specific organelle, and fluorescence intensity of the two organelles for the analysis of morphological modifications were evaluated by eye by two evaluators. The differences in terms of morphology (signal vs. reduction/absence of signal for a given organelle) between treated and untreated parasites were analysed for statistical significance based on the total number of parasites that were observed for each category using Fisher's exact test in Prism 10 (GraphPad).

Cytotoxicity assays with the rat L6 cell line.

Cytotoxicity was determined in vitro against rat L6 myoblasts as described earlier (50). Cell proliferation was assessed with resazurin, and the generally cytotoxic agent podophyllotoxin served as the positive control.

***Toxoplasma gondii* assays and bioimaging**

Parasite culture. Type I *T. gondii* tachyzoites (RH strain, ref. 51) were maintained by serial passage in human foreskin fibroblast (HFF, American Type Culture Collection, CRL 1634) cell monolayer grown in Dulbecco's modified Eagle medium (supplemented with 5% decomplemented fetal bovine serum, 2-mM l-glutamine and a cocktail of penicillin-streptomycin (Gibco) at 100 µg/ml).

Plaque assays and IC_{50} calculations. Confluent monolayers of HFFs were infected with freshly egressed parasites, which were left to grow for 7 days in the presence of compound (added to various final concentrations), or with the vehicle only (DMSO, whose added volume corresponded to the highest concentration of compound). Cells were then fixed with 4% v/v PFA and plaques were revealed by staining with a 0.1% crystal violet solution (V5265, Sigma-Aldrich). Images were acquired with an Olympus MVX10 macro zoom microscope equipped with an Olympus XC50 camera. Plaque area measurements were done using ZEN software (Zeiss). Plaque areas from three independent biological replicates were plotted relative to compound concentrations and IC_{50} values using a nonlinear regression model software (Graphpad Prism 8).

Immunofluorescence assays. Immunofluorescence assays (IFA) were performed as described previously (52). Briefly, intracellular tachyzoites grown on coverslips containing HFF monolayers, were fixed for 20 min with 4% (w/v) paraformaldehyde in PBS and permeabilized for 10 min with 0.3% Triton X-100 in PBS. Coverslips were subsequently blocked with 0.1% (w/v) BSA in PBS and primary antibodies used (at 1/1,000) to detect subcellular structures were rabbit anti-IMC3 (53) to outline the parasite shape, rabbit anti-pyruvate dehydrogenase-

E2 (35) to detect the apicoplast, and mouse anti-F1-ATPase beta subunit (kind gift of P. Bradley, UCLA) to detect the mitochondrial network. The differences between treated and untreated parasites were analysed for statistical significance based on the total number of parasites that were observed for each category using Fisher's exact test in Prism 10 (GraphPad).

Lipidomic profile of neosynthesized fatty acids in the apicoplast of *T. gondii* tachyzoites under drug treatment.

Total lipid analysis: Total lipids were extracted in chloroform/methanol/water (1:3:1, v/v/v) containing FFA (free fatty acids C13:0, 10 nmol) and PC (21:0/21:0, 10 nmol) as internal standards for extraction. Next, the polar and apolar metabolites were separated by phase partitioning by adding chloroform and water to give the ratio of chloroform/methanol/water as 2:1:0.8 (v/v/v). For lipid analysis, 50 μ L of the extract was directly dried and dissolved in 2:1 chloroform:methanol and trimethylsulfonium hydroxide (TMSH, Macherey Nagel) for total fatty acid content. Resultant FAMES were then analyzed by GC-MS as previously described (33,34,54). All FAMES were identified by comparison of retention time and mass spectra from GC-MS with authentic chemical standards. The concentration of FAMES was quantified after initial normalization to different internal standards.

Tracking FASII origin fatty acids (monitoring de novo FA synthesis by the parasite apicoplast FASII). Treated or untreated parasites were infected to a confluent monolayer of HFF in glucose-free-DMEM (1% FBS) supplemented with U-¹³C-glucose or U-¹²C-glucose at a final concentration of 800 μ M, with or without ATc (0.5 μ gml⁻¹). The parasites were harvested up to 48 h post treatment and metabolically quenched in a dry ice and ethanol slurry in a tube until the sample reached 4 °C. Lipids were extracted, derivatized using TMSH (Macherey-Nagel) and analyzed by GC-MS as described above. ¹³C incorporation to each fatty acid was calculated as the percent of the metabolite pool containing one or more ¹³C atoms after correction for natural abundance and the amount of ¹³C-carbon source in the culture medium. Isotopomers (isotopic isomers) are molecular species from the same metabolite that are compositionally identical but are constitutionally and/or stereochemically isomeric because of isotopic substitution (55) (i.e. the presence of ¹³C stable isotope(s) instead of naturally occurring ¹²C isotope in the FA molecule in our case). The degree of the incorporation of ¹³C into fatty acids (% carbon incorporation) was determined by the mass isotopomer distribution (MID) of each FAMES. MID was obtained from the shift in isotopic mass dependent on the amount of ¹²C carbons compared to the integration of ¹³C carbon atoms. The total abundance of ¹³C-labeled fatty acids was obtained by calculating the concentration of all isotopomers of ¹³C-labeled FAMES and finally normalizing to authentic internal standards and parasite number. Differences between treated and untreated parasites were analysed using a t-test for each lipidomic analysis (GraphPad Prism 10).

Fluorescence imaging of the compounds using click-chemistry in *Toxoplasma*.

Intracellular parasites were incubated with the alkyne derivatives of 3-benzyl-menadiones at 10 μ M for 6 h. They were then fixed with 4% (w/v) paraformaldehyde in PBS and permeabilized for 10 min with 0.3% Triton X-100 in PBS, before performing the click reaction with Alexa Fluor 488 Azide (ThermoFisher ref. A10266) and the "Click-it" Cell Reaction Buffer Kit (ThermoFisher ref. A10269) according to the conditions suggested by the manufacturer. Briefly, the click reaction was performed for 30 min at room temperature with 5 μ M of Alexa Fluor 488 Azide in the presence of CuSO₄, and for co-staining with the apicoplast marker, the samples were then processed for IFA as described above. Colocalized signals were scored by eye, based on image superimposition and the analysis of dual color fluorescence images for colocalized pixels.

Ecotoxicity Assays

Desmodesmus subspicatus assays

***Desmodesmus* culture.** The algae *D. subspicatus* (SAG 86.81; Culture Collection of Algae, Göttingen University, Germany) were maintained in a climate-controlled cabinet (SANZO; EWALD Innovationstechnik GmbH, Germany) at a temperature of $21 \pm 1^\circ\text{C}$ with a light:dark photoperiod of 16:8 hours (5000-5500 lux; cool-white illumination). The culture was grown in a nutrient medium (56) and subjected to continuous stirring at a rate of 250 rpm while receiving constant aeration.

For the inoculum culture of *D. subspicatus* used in the subsequent toxicity tests, a preparation was made three days prior to the start of each test, carried out in the same nutrient medium (56). To achieve this, 5 mL of the algae solution were transferred into 5 L of Kuhl-medium and placed in a climate-controlled cabinet at $21 \pm 1^\circ\text{C}$, with constant illumination and stirring.

***Desmodesmus* growth inhibition testing.** During a series of acute toxicity tests, *Desmodesmus* algae were exposed to three test substances, namely **PD**, **3b**, and **3i**. In short, the test medium used was Kuhl-medium, and each acute toxicity test followed the OECD guideline 201 (57) for a duration of up to 96 h (for specific test concentrations see Table 5). In each microcosm ($n=3$), the initial biomass of algae did not exceed 0.5 mg dry weight *per* liter, and the initial cell concentration ranged from 2.0 to 5.0×10^3 cells/mL. The microcosms were sealed with cotton caps to prevent the entry of dust while allowing for gas exchange. These microcosms were maintained in a climate-controlled cabinet under the conditions mentioned earlier. Every 24 hours, the number of algal cells in the microcosms was quantified using relative fluorescence units, measured with a multiplate reader (Tecan Infinite® M200, Tecan Group Ltd., Switzerland) using excitation and emission wavelengths at 420 nm and 670 nm, respectively. Relative fluorescence units were converted to cell numbers *per* mL using pre-established calibration curves.

Daphnia magna assays

***Daphnia* culture.** *Daphnia magna* (Clone V; Eurofins-GAB, Niefern-Oeschelbronn, Germany) were maintained as a permanent culture in a climate-controlled room at a temperature of $20 \pm 1^\circ\text{C}$ with a 16:8 h light:dark photoperiod (800-1000 lux; OSRAM L 58W/21-840 ECO, Germany). Reconstituted hard water was used as medium, prepared following the guidelines for conducting acute toxicity tests outlined in ASTM (58). The medium was supplemented with vitamins (biotin, thiamine, cyanocobalamin; as *per* OECD (2004), selenium, and 20 $\mu\text{L/L}$ of Seaweed (equivalent to 8 mg total organic carbon/L; Marinure®, Glenside, Scotland). Until the start of the toxicity tests, the medium was replaced three times *per* week and organisms were fed daily with the alga *D. subspicatus* in a size-dependent manner at an equivalent of 66-100 $\mu\text{g C/animal}$.

***Daphnia* immobility testing.** During a series of acute toxicity tests, *Daphnia* were exposed to three test substances, namely **PD**, **3b**, and **3i**. In short, the test medium used was ASTM reconstituted hard water; however, food or seaweed supplements were not added. Each acute toxicity test followed the OECD guideline 202 (OECD, 2004) but the study duration was extended to 96 hours. In each replicate ($n=4$), five juvenile *Daphnia* (less than 24 h-old) were subjected to increasing concentrations of the test substances, and their immobility was assessed as an indicator of toxicity every 24 hours (for specific test concentrations see Table 5). All tests were conducted under the same temperature and light conditions as previously described.

Table 5. Concentrations of the test items used in toxicity tests with *D. subspicatus* and *D. magna*.

Test item	Test organism	Concentrations tested (μM)
PD	<i>D. subspicatus</i>	0, 0.0625, 0.125, 0.25, 0.5, 1
	<i>D. magna</i>	0, 31.25, 62.5, 125, 250, 500, 1000
3b	<i>D. subspicatus</i>	0, 0.0625, 0.125, 0.25, 0.5, 1
	<i>D. magna</i>	0, 0.21875, 0.4375, 0.875, 1.75, 3.5, 7
3i	<i>D. subspicatus</i>	0, 0.0625, 0.125, 0.25, 0.5, 1
	<i>D. magna</i>	0, 0.625, 1.25, 2.5, 5, 10, 20

Data evaluation. For acute toxicity tests with *Desmodesmus* and *Daphnia*, effective concentrations of the test item causing 10%, 20%, and 50% in the test organisms (i.e., EC10, EC20, and EC50, respectively) were determined after 96 h of exposure using the statistical software R (59). Several dose-response models (always with lower limit at 0) were used to fit the data using the R package “drm” (60) and the models fitting the data best were selected based on visual judgement and Akaike’s information criterion.


■ ASSOCIATED CONTENT

The Supporting Information is available free of charge at <https://pubs.acs.org/doi/>

Supporting Information (ESI) content: Procedures and additional data: pages S2-S3 – anti-*T. gondii* activity of the selected compounds in plaque assays for evaluating the lytic cycle of *Toxoplasma gondii* (Figure S1) and IC₅₀ curves based on plaque area (Figure S2); pages S4-S7 – lipidomics data (Figures S3-S10); pages S8-S9 – Stability of azido derivative **16** (Figures S11-S13); page S10 – Subcellular localization of probe **3v** in asexual blood stages of *P. falciparum* (trophozoite stage) after 2 h of incubation (Figure S14) ; page S11 – Subcellular localization of probe **8** in asexual blood stages of *P. falciparum* (trophozoite stage) after 2 h of incubation (Figure S15) ; pages S12-S13 – Parasite and vacuole counts for apicoplast loss and parasite counts for mitochondrial morphology in *T. gondii* (Table S1-S3); page S14 – Morphological analysis of *P. falciparum* parasites for the presence of mitochondria and apicoplast upon treatment with PD or probe **8** (50 nM) and in untreated control parasites (Table S1) ; pages S15-S68 – ¹H, ¹⁹F and ¹³C {¹H} NMR spectra of compounds **1–16**. (PDF)

■ AUTHOR INFORMATION

Corresponding Author

Elisabeth Davioud-Charvet – UMR7042 CNRS-Unistra-UHA, Laboratoire d’Innovation Moléculaire et Applications (LIMA), Bio(in)organic & Medicinal Chemistry Team, European school of Chemistry, Polymers and Materials (ECPM), 25, rue Becquerel, F-67087 Strasbourg, France;  orcid.org/0000-0001-7026-4034; Phone: +33 (0)3.20.68.85.26.20.; Email: elisabeth.davioud@unistra.fr

Authors


Baptiste Dupouy, Maxime Donzel, Matthieu Roignant – CNRS-Université de Strasbourg-Université Haute-Alsace UMR7042, Laboratoire d'Innovation Moléculaire et Applications (LIMA), Team Bio(IN)organic & Medicinal Chemistry, European School of Chemistry, Polymers and Materials (ECPM), 25, rue Becquerel, F-67087 Strasbourg, France;


Yann Bordat, Sébastien Besteiro – UMR5294 CNRS-Université de Montpellier, Laboratory of Pathogens and Host Immunity (LPHI), Place Eugène Bataillon, Bâtiment 24, CC 107, 34095 Montpellier cedex 5, France

Sarah Charital, Yoshiki Yamaro-Botté, Cyrille Y. Botté – UMR5309 CNRS INSERM UGA, ApicoLipid Group, IAB Institut Jean Roget, Domaine de la Merci, 38700 La Tronche, France

Rodrigue Keumoe, Stéphanie A. Blandin – INSERM, CNRS, Université de Strasbourg, U1257 / UPR9022, Mosquito Immune Responses, IBMC, 2 Allée Konrad Roentgen, F-67000 Strasbourg, France ; orcid.org/0000-0003-4566-1200

Matthias Rottmann, Pascal Mäser – Swiss Tropical and Public Health Institute, Department of Medical Parasitology and Infection Biology, CH-4123 Allschwil, Switzerland; University of Basel, CH-4003 Basel, Switzerland

Pascal Mäser – University of Basel, CH-4003 Basel, Switzerland;  orcid.org/0000-0003-3122-1941.

Alexander Feckler, Mirco Bundschuh – Functional Aquatic Ecotoxicology, Institute for Environmental Sciences (iES), RPTU Kaiserslautern-Landau, Fortstrasse 7, 76829 Landau, Germany;  orcid.org/0000-0003-4876-220X

Author Contributions

B.D., M.D., M.R. synthesized the compounds described in this present work; Y. B., C. S., Y. Y.-B., R. K., R. M. and P.R., M.B. and A.F. generated and analyzed data. E.D.C., S.A.B., S.B., C.B. analyzed the data and wrote the paper.

Notes

The authors declare no competing financial interest.

■ ACKNOWLEDGMENTS

E.D.-C., S.A.B., C.Y.B., and S.B. wish to thank the Laboratoire d'Excellence (LabEx) ParaFrap [ANR-11-LABX-0024], for funding, providing B.D.'s PhD salary, and for initiating and fostering this scientific research and collaboration. This work was furthermore supported by the European Campus EUCOR, via the seed-money program ("ROSkillers" project, E.D.-C., S.A.B., M.R., P.M.) between Strasbourg and Basel Universities, and the Agence Nationale de la Recherche, France (Program ANR-PRCI with FNS, Project "ROSaction", grant ANR-22-CE93-0005-01 to E.D.-C., S.A.B., M.R., P.M.; Program ANR-PRC, project "PlasmoPrim", grant ANR-17-CE15-0013-01 to E.D.-C., S.A.B., including Ph.D. student salary to M.D.), the CNRS innovation (Program maturation, project "ROS-palu" to E.D.-C., S.A.B., including postdoc salary to M.R.). C.Y.B., Y.Y.B., and S.C. were supported by Agence Nationale de la Recherche, France (Project ApicoLipidAdapt grant ANR-21-CE44-0010, Project Apicolipidtraffic grant ANR-23-CE15-0009-01), the Fondation pour la Recherche Médicale (FRM EQU202103012700), LIA-IRP CNRS Program (Apicolipid project), the Université Grenoble Alpes (IDEX ISP-IRGA Apicolipid), Région Auvergne Rhone-Alpes for the lipidomics analyses platform (Grant IRICE Project GEMELI), the CEFIPRA via a Collaborative Research Program Grant (Project 6003-1). We are grateful to the IBMC Insectary platform which is part of and supported by several networks (CORTECS, IBiSA and Emerg'In), and to Jean Daniel Fauny and Romain Vauchelle from the IBMC Microscopy Platform for their training and guidance in fluorescence microscopy. We acknowledge the IBMP Cell Imaging Facility, member of the national infrastructure France-BioImaging supported by the French National Research Agency (ANR-10-INBS-04) for image acquisitions. The laboratories also receive support from CNRS (E.D.-C., and S.A.B.), Inserm (S.A.B.) and from the University of Strasbourg (E.D.-C., S.A.B.).

■ ABBREVIATIONS

BCl₃ = boron trichloride; CuAAC = Copper(I) catalyzed Azide-Alkyne Cycloaddition; DCM = dichloromethane; FAs = fatty acids; MeOH = methanol; m.p. = melting point; NEt₃ or TEA = triethylamine; rt = room temperature; TBAI = tetra-n-butylammonium iodide; CHX = cyclohexane; T = toluene; EtOAc = ethyl acetate; AcOH = acetic acid.

■ REFERENCES

- (1) WHO malaria report 2023 for the year 2022.
- (2) Rosenthal, P. J.; Asua, V.; Bailey, J. A.; Conrad, M. D.; Ishengoma, D. S.; Kanya, M. R.; Rasmussen, C.; Tadesse, F. G.; Uwimana, A.; Fidock, D. A. The emergence of artemisinin partial resistance in Africa: how do we respond? *Lancet Infect Dis.* **2024**, S1473-3099(24)00141-5.
- (3) Müller, T.; Johann, L.; Jannack, B.; Brückner, M.; Lanfranchi, D. A.; Bauer, H.; Sanchez, C.; Yardley, V.; Deregnaucourt, C.; Schrével, J.; Lanzer, M.; Schirmer, R. H.; Davioud-Charvet, E. Glutathione reductase-catalyzed cascade of redox reactions to bioactivate potent antimalarial 1,4-

- naphthoquinones – A new strategy to combat malarial parasites. *J. Am. Chem. Soc.* **2011**, *133*, 11557-11571.
- (4) Ehrhardt, K.; Deregnacourt, C.; Goetz, A.-A.; Tzanova, T.; Pradines, B.; Adjalley, S. H.; Blandin, S.; Bagrel, D.; Lanzer, M.; Davioud-Charvet, E. The redox-cycler plasmodione is a fast acting antimalarial lead compound with pronounced activity against sexual and early asexual blood-stage parasites. *Antimicrob. Agents Chemother.* **2016**, *60*, 5146-5158.
 - (5) Bielitz, M.; Belorgey, D.; Ehrhardt, K.; Johann, L.; Lanfranchi, D. A.; Gallo, V.; Schwarzer, E.; Moring, F.; Jortzik, E.; Williams, D. L.; Becker, K.; Arese, P.; Elhabiri, M.; Davioud-Charvet E. Antimalarial NADPH-consuming redox-cyclers as superior G6PD deficiency copycats. *Antioxid. Redox Signal.* **2015**, *22*, 1337-1351.
 - (6) Cotos, L.; Donzel, M.; Elhabiri, M.; Davioud-Charvet, E. A mild and versatile Friedel-Crafts methodology for the diversity-oriented synthesis of redox-active 3-benzoylmenadiones with tuneable redox potentials. *Chemistry* **2020**, *26*, 3314-3325.
 - (7) Cichocki, B.; Donzel, M.; Heimsch, K. C.; Lesanavičius, M.; Feng, L.; Montagut, E. J.; Becker, K.; Aliverti, A.; Elhabiri, M.; Cenas, N.; Davioud-Charvet, E. *Plasmodium falciparum* ferredoxin-NADP⁺ reductase-catalyzed redox cycling of plasmodione generates both predicted key drug metabolites: Implication for antimalarial drug development. *ACS Infect. Dis.* **2021**, *7*, 1996-2012.
 - (8) Johann, L.; Lanfranchi, D. A.; Davioud-Charvet, E.; Elhabiri, M. A physico-biochemical study on potential redox-cyclers as antimalarial and anti-schistosomal drugs. *Curr. Pharm. Des.* **2012**, *18*, 3539-3566.
 - (9) Elhabiri, M.; Sidorov, P.; Cesar-Rodo, E.; Marcou, G.; Lanfranchi, D. A.; Davioud-Charvet, E.; Horvath, D.; Varnek, A. Electrochemical properties of substituted 2-methyl-1,4-naphthoquinones: redox behavior predictions. *Chemistry* **2015**, *21*, 3415-3424.
 - (10) Sidorov, P.; Desta, I.; Chessé, M.; Horvath, D.; Marcou, G.; Varnek, A.; Davioud-Charvet, E.; Elhabiri, M. Redox polypharmacology is an emerging strategy to combat malarial parasites. *ChemMedChem* **2016**, *11*, 1339–1351.
 - (11) Mounkoro, P.; Michel, T.; Blandin, S.; Golinelli-Cohen, M.-P.; Davioud-Charvet, E.; Meunier, B. Investigating the mode of action of the redox-active antimalarial drug plasmodione using the yeast model. *Free Radic. Biol. Med.* **2019**, *141*, 269–278.
 - (12) Mounkoro, P.; Michel, T.; Golinelli-Cohen, M.-P.; Blandin, S.; Davioud-Charvet, E.; Meunier, B. A role for the succinate dehydrogenase in the mode of action of the redox-active antimalarial drug, plasmodione. *Free Radic. Biol. Med.* **2021**, *162*, 533-541.
 - (13) Feng, L.; Lanfranchi, D. A.; Cotos-Munoz, L.; Cesar Rodo, E.; Ehrhardt, K.; Goetz, A.-A.; Zimmerman, H.; Fenaille, F.; Blandin, S.; Davioud-Charvet, E. Synthesis of plasmodione metabolites and ¹³C-enriched plasmodione as chemical tools for drug metabolism investigation. *Org. Biomol. Chem.* **2018**, *16*, 2647-2665.
 - (14) Cichocki, B.; Khobragade, V.; Donzel, M.; Cotos, L.; Blandin, S.; Schaeffer-Reiss, C.; Cianféroni, S.; Strub, J.-M.; Elhabiri, M.; Davioud-Charvet, E. A new class of valuable (pro-)activity-based protein profiling probes: application to the redox-active antimalarial drug, plasmodione. *JACS^{au}* **2021**, *1*, 669-689.
 - (15) Fienberg, S.; Eyer mann, C. J.; Arendse, L. B.; Basarab, G. S.; McPhail, J. A.; Burke, J. E.; Chibale, K. Structural Basis for Inhibitor Potency and Selectivity of *Plasmodium falciparum* Phosphatidylinositol 4-Kinase Inhibitors. *ACS Infect. Dis.* **2020**, *6*, 3048-3063.
 - (16) Mehta, N., Ferrins, L., Leed, S. E., Sciotti, R. J., Pollastri, M. P. Optimization of Physicochemical Properties for 4-Anilinoquinoline Inhibitors of *Plasmodium falciparum* Proliferation. *ACS Infect. Dis.* **2018**, *4*, 577-591.
 - (17) Meanwell, N. A. Chapter Five - A Synopsis of the Properties and Applications of Heteroaromatic Rings in Medicinal Chemistry. *Adv. Heterocycl. Chem.* **2017**, *123*, 245-361.
 - (18) Lanfranchi, D. A.; Cesar-Rodo, E.; Bertrand, B.; Huang, H.-H.; Day, L.; Johann, L.; Elhabiri, M.; Becker, K.; Williams, D. L.; Davioud-Charvet, E. Synthesis and biological evaluation of 1,4-naphthoquinones and quinoline-5,8-diones as antimalarial and schistosomicidal agents. *Org. Biomol. Chem.* **2012**, *10*, 6375-6387.
 - (19) Kim, K.; Weiss, L. M. *Toxoplasma gondii*: the model apicomplexan. *Int. J. Parasitol.* **2004**, *34*, 423-432.
 - (20) Sanchez, S. G., Besteiro, S. The pathogenicity and virulence of *Toxoplasma gondii*. *Virulence* **2021**, *12*, 3095-3114.

- (21) Uteuliyev, M. M.; Shu, L.; Richards, S. J.; Warkentin, A. A.; Davis, D. Naphthoquinone derivatives for treatment of oxidative stress disorders and their preparation. PTC Therapeutics, Inc. World Intellectual Property Organization, WO2020252414 A1, 2020-12-17
- (22) Cox, P. A.; Leach, A. G.; Campbell, A. D.; Lloyd-Jones, G. C. Protodeboronation of Heteroaromatic, Vinyl, and Cyclopropyl Boronic Acids: pH-Rate Profiles, Autocatalysis, and Disproportionation. **J Am Chem Soc.** **2016**, *138*, 9145-9157.
- (23) Hajipour, A. R.; Mohammadsaleh, F. Preparation of Aryl Azides from Aromatic Amines in N-Methyl-2-Pyrrolidonium Bisulfate. **Org. Prep. Proced. Int.** **2011**, *43*, 451-455.
- (24) Snyder, C.; Chollet, J.; Santo-Tomas, J.; Scheurer, C.; Wittlin S. In vitro and in vivo interaction of synthetic peroxide RBx11160 (OZ277) with piperazine in *Plasmodium* models. **Exp. Parasitol.** **2007**, *115*, 296-300.
- (25) Araujo, F. G.; Huskinson, J.; Remington, J. S. Remarkable in Vitro and in Vivo Activities of the Hydroxynaphthoquinone 566C80 against Tachyzoites and Tissue Cysts of *Toxoplasma Gondii*. **Antimicrob. Agents Chemother.** **1991**, *35*, 293–299.
- (26) Fleige, T.; Fischer, K.; Ferguson, D. J.; Gross, U.; Bohne, W. Carbohydrate metabolism in the *Toxoplasma gondii* apicoplast: localization of three glycolytic isoenzymes, the single pyruvate dehydrogenase complex, and a plastid phosphate translocator. **Eukaryot. Cell.** **2007**, *6*, 984-996.
- (27) Huet, D., Rajendran, E., van Dooren, G. G., Lourido, S. Identification of cryptic subunits from an apicomplexan ATP synthase. **Elife** **2018**, *7*:e38097.
- (28) Ovcariikova, J.; Lemgruber, L.; Stilger, K. L.; Sullivan, W. J.; Sheiner, L. Mitochondrial Behaviour throughout the Lytic Cycle of *Toxoplasma gondii*. **Sci. Rep.** **2017**, *7*, 42746.
- (29) Botté C. Y., Dubar F., McFadden G.I., Maréchal E., Biot C. *Plasmodium falciparum* apicoplast drugs: targets or off-targets? **Chem Rev.** **2012**, *112*, 1269-1283.
- (30) Waller, R. F.; Ralph, S. A.; Reed, M. B.; Su, V.; Douglas, J. D.; Minnikin, D. E.; Cowman, A. F.; Besra, G. S.; McFadden, G. I. A type II pathway for fatty acid biosynthesis presents drug targets in *Plasmodium falciparum*. **Antimicrob. Agents Chemother.** **2003**, *47*, 297-301.
- (31) Ramakrishnan, S.; Docampo, M. D.; Macrae, J. I.; Pujol, F. M.; Brooks, C. F.; van Dooren, G. G.; Hiltunen, J. K.; Kastaniotis, A. J.; McConville, M. J.; Striepen, B. Apicoplast and endoplasmic reticulum cooperate in fatty acid biosynthesis in apicomplexan parasite *Toxoplasma gondii*. **J. Biol. Chem.** **2012**, *287*, 4957-4971.
- (32) Amiar, S.; MacRae, J. I.; Callahan, D. L.; Dubois, D.; van Dooren, G. G.; Shears, M. J.; Cesbron-Delauw, M. F.; Maréchal, E.; McConville, M. J.; McFadden, G. I.; Yamaryo-Botté, Y.; Botté, C. Y. Apicoplast-Localized Lysophosphatidic Acid Precursor Assembly Is Required for Bulk Phospholipid Synthesis in *Toxoplasma gondii* and Relies on an Algal/Plant-Like Glycerol 3-Phosphate Acyltransferase. **PLoS Pathog.** **2016**, *12*, e1005765.
- (33) Amiar, S.; Katris, N. J.; Berry, L.; Dass, S.; Duley, S.; Arnold, C. S.; Shears, M. J.; Brunet, C.; Touquet, B.; McFadden, G.I.; Yamaryo-Botté, Y.; Botté, C. Y. Division and Adaptation to Host Environment of Apicomplexan Parasites Depend on Apicoplast Lipid Metabolic Plasticity and Host Organelle Remodeling. **Cell Rep.** **2020**, *30*, 3778-3792.e9.
- (34) Dass, S.; Shunmugam, S.; Berry, L.; Arnold, C. S.; Katris, N. J.; Duley, S.; Pierrel, F.; Cesbron-Delauw, M. F.; Yamaryo-Botté, Y.; Botté, C. Y. *Toxoplasma* LIPIN is essential in channeling host lipid fluxes through membrane biogenesis and lipid storage. **Nat. Commun.** **2021**, *12*, 2813.
- (35) Renaud, E. A.; Pamukcu, S.; Cerutti, A.; Berry, L.; Lemaire-Vieille, C.; Yamaryo-Botté, Y.; Botté, C. Y.; Besteiro, S. disrupting the plastidic iron-sulfur cluster biogenesis pathway in *Toxoplasma gondii* has pleiotropic effects irreversibly impacting parasite viability. **J. Biol. Chem.** **2022**, *298*, 102243.
- (36) Kennedy, K.; Crisafulli, E. M.; Ralph, S. A. Delayed Death by Plastid Inhibition in Apicomplexan Parasites. **Trends Parasitol.** **2019**, *35*, 747-759.
- (37) Kennedy, K.; Cobbold, S. A.; Hanssen, E.; Birnbaum, J.; Spillman, N. J.; McHugh, E.; Brown, H.; Tilley, L.; Spielmann, T.; McConville, M. J.; Ralph, S. A. Delayed death in the malaria parasite *Plasmodium falciparum* is caused by disruption of prenylation-dependent intracellular trafficking. **PLoS Biol.** **2019**, *17*, e3000376.
- (38) Amrane, D.; Primas, N.; Arnold, C. S.; Hutter, S.; Louis, B.; Sanz-Serrano, J.; Azqueta, A.; Amanzougaghene, N.; Tajeri, S.; Mazier, D.; Verhaeghe, P.; Azas, N.; Botté, C.; Vanelle, P. Antiplasmodial 2-thiophenoxy-3-trichloromethyl quinoxalines target the apicoplast of *Plasmodium falciparum*. **Eur J Med Chem.** **2021**, *224*, 113722.

- (39) Charital, S.; Lourdel, A.; Quansah, N.; Botté, C. Y.; Yamaryo-Botté, Y. Monitoring of Lipid Fluxes Between Host and Plastid-Bearing Apicomplexan Parasites. *Methods Mol. Biol.* 2024, 2776, 197-204.
- (40) Brooks, C. F.; Johnsen, H.; van Dooren, G. G.; Muthalagi, M.; Lin, S. S.; Bohne, W.; Fischer, K.; Striepen, B. The toxoplasma apicoplast phosphate translocator links cytosolic and apicoplast metabolism and is essential for parasite survival. *Cell Host Microbe* 2010, 7, 62-73.
- (41) Iacobucci, I.; Monaco, V.; Dupouy, B.; Hovasse, A.; Keumoe, R.; Cichocki, B.; Elhabiri, M.; Blandin, S. A.; Meunier, B.; Strub, J.-M.; Monti, M.; Cianféroni, S.; Schaeffer-Reiss, C.; Davioud-Charvet, E. Proteomic profiling of antimalarial plasmodione using 3-benz(o)ylmenadione affinity-based probes. *ChemBioChem* 2024, 2024, 25(15):e202400187.
- (42) Lesanavičius, M.; Aliverti, A.; Šarlauskas, J.; Čėnas, N. Reactions of Plasmodium falciparum Ferredoxin:NADP+ Oxidoreductase with Redox Cycling Xenobiotics: A Mechanistic Study. *Int. J. Mol. Sci.* 2020, 21, 3234.
- (43) Staines, H. M.; Ellory, J. C.; Chibale, K. The new permeability pathways: targets and selective routes for the development of new antimalarial agents. *Comb. Chem. High Throughput Screen.* 2005, 8, 81-88.
- (44) Henry, N.; Enguehard-Gueiffier, C.; They, I.; Gueiffier, A. One-Pot Dual Substitutions of Bromobenzyl Chloride, 2-Chloromethyl-6-halogenoimidazo[1,2-a]pyridine and -[1,2-b]pyridazine by Suzuki–Miyaura Cross-Coupling Reactions. *Eur. J. Org. Chem.* 2008, 2008, 4824-4827.
- (45) Schlosser, M.; Cottet, F. Silyl-Mediated Halogen/Halogen Displacement in Pyridines and Other Heterocycles. *Eur. J. Org. Chem.* 2002, 2002, 4181-4184.
- (46) Šturala, J.; Boháčová, S.; Chudoba, J.; Metelková, R.; Cibulka, R. Electron-Deficient Heteroarenium Salts: An Organocatalytic Tool for Activation of Hydrogen Peroxide in Oxidations. *J. Org. Chem.* 2015, 80, 2676–2699.
- (47) Desjardins, R. E.; Canfield, C. J.; Haynes, J. D.; Chulay, J. D. Quantitative assessment of antimalarial activity in vitro by a semiautomated microdilution technique. *Antimicrob. Agents Chemother.* 1979, 16, 710-718.
- (48) Tonkin, C. J.; Van Dooren, G. G.; Spurck, T. P.; Struck, N. S.; Good, R. T.; Handman, E.; Cowman, A. F.; McFadden, G. I. Localization of Organellar Proteins in Plasmodium Falciparum Using a Novel Set of Transfection Vectors and a New Immunofluorescence Fixation Method. *Mol. Biochem. Parasitol.* 2004, 137, 13–21.
- (49) Agrawal, S.; Van Dooren, G. G.; Beatty, W. L.; Striepen, B. Genetic Evidence That an Endosymbiont-Derived Endoplasmic Reticulum-Associated Protein Degradation (ERAD) System Functions in Import of Apicoplast Proteins. *J. Biol. Chem.* 2009, 284, 33683–33691.
- (50) Bernal, F. A.; Kaiser, M.; Wünsch, B.; Schmidt, T. J. Structure-Activity Relationships of Cinnamate Ester Analogues as Potent Antiprotozoal Agents. *ChemMedChem.* 2020, 15, 68-78.
- (51) Sabin, A. B. Toxoplasmic Encephalitis in Children. *JAMA* 1941, 116, 801.
- (52) Semenovskaya, K.; Lévêque, M. F.; Berry, L.; Bordat, Y.; Dubremetz, J.; Lebrun, M.; Besteiro, S. TgZFP2 Is a Novel Zinc Finger Protein Involved in Coordinating Mitosis and Budding in Toxoplasma. *Cell. Microbiol.* 2020, 22, e13120.
- (53) Anderson-White, B. R.; Ivey, F. D.; Cheng, K.; Szatanek, T.; Lorestani, A.; Beckers, C. J.; Ferguson, D. J. P.; Sahoo, N.; Gubbels, M.-J. A Family of Intermediate Filament-like Proteins Is Sequentially Assembled into the Cytoskeleton of Toxoplasma gondii. *Cell. Microbiol.* 2011, 13, 18–31.
- (54) Dubois, D.; Fernandes, S.; Amiar, S.; Dass, S.; Katris, N. J.; Botté, C. Y.; Yamaryo-Botté, Y. Toxoplasma gondii acetyl-CoA synthetase is involved in fatty acid elongation (of long fatty acid chains) during tachyzoite life stages. *J. Lipid Res.* 2018, 59, 994-1004.
- (55) Stoll S. Isotopomers and Isotopologues: The History behind the Confusion. *Chem. Educator* 2007, 12, 1–3.
- (56) Kuhl, A.; Lorenzen, H. Handling and culturing of Chlorella. *Methods in cell physiology* 1964, 1, 159-187, Prescott, DM, ed.
- (57) OECD. OECD Guidelines for the testing of chemicals. Test Guideline 201: freshwater alga and cyanobacterial, growth inhibition test. Organisation for Economic Co-operation and Development, Paris; 2011.
- (58) ASTM Standard E729. Standard guide for conducting acute toxicity tests on test materials with fishes, macroinvertebrates, and amphibian; 2007.

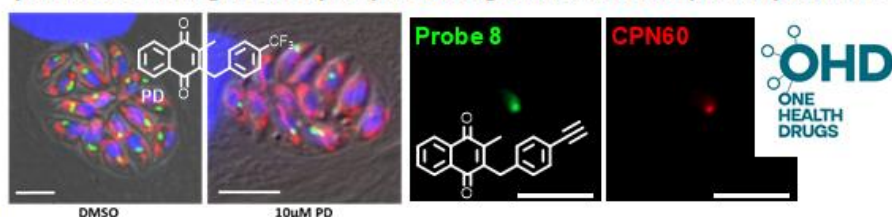
- (59) R Core Team. R: a language and environment for statistical computing, version 4.3.1. R Foundation for Statistical Computing. Vienna, Austria; **2023**. [https:// www.R-project.org/](https://www.R-project.org/)
- (60) Ritz, C.; Baty, F.; Streibig, J. C.; Gerhard, D. Dose-response analysis using R. ***PLoS One*** **2015**, *10*, e0146021.

TOC graphic "For Table of Contents Use Only"

3-benzylmenadiones and their heteroaromatic analogues target the apicoplast of Apicomplexa parasites: Synthesis and bioimaging studies

Baptiste Dupouy,^{1,#} Maxime Donzel,^{1,#} Matthieu Roignant,^{1,#} Sarah Charital,² Rodrigue Keumoe,³ Yoshiki Yamaryo-Botté,² Alexander Feckler,⁴ Mirco Bundschuh,⁴ Yann Bordat,⁵ Matthias Rottmann,⁶ Pascal Mäser,^{6,7} Cyrille Y. Botté,² Stéphanie A. Blandin,³ Sébastien Besteiro,⁵ Elisabeth Davioud-Charvet*,¹

plasmodione targets the apicoplast of *T. gondii* and *P. falciparum* parasites



¹ UMR7042 CNRS-Unistra-UHA, Laboratoire d'Innovation Moléculaire et Applications (LIMA), Bio(in)organic & Medicinal Chemistry Team, European school of Chemistry, Polymers and Materials (ECPM), 25, rue Becquerel, F-67087 Strasbourg, France.

² Apicolipid Team, Institut pour l'Avancée des Biosciences, CNRS UMR5309,INSERM U1209, Université Grenoble Alpes, Bat. Jean Roget, Domaine de la Merci, F-38700 La Tronche, France.

³ INSERM, CNRS, Université de Strasbourg, U1257 / UPR9022, Mosquito Immune Responses IBMC, 2 Allée Konrad Roentgen, F-67000 Strasbourg, France.

⁴ Functional Aquatic Ecotoxicology, Institute for Environmental Sciences (iES), RPTU Kaiserslautern-Landau, Fortstrasse 7, D-76829 Landau, Germany

⁵ UMR5294 CNRS-Université de Montpellier, Laboratory of Pathogens and Host Immunity (LPHI), Place Eugène Bataillon, Bâtiment 24, CC 107, F-34095 Montpellier cedex 5, France.

⁶ Swiss Tropical and Public Health Institute, Kreuzstrasse 2, CH-4123 Allschwil, Switzerland.

⁷ University of Basel, Petersgraben 1, CH-4001 Basel, Switzerland.